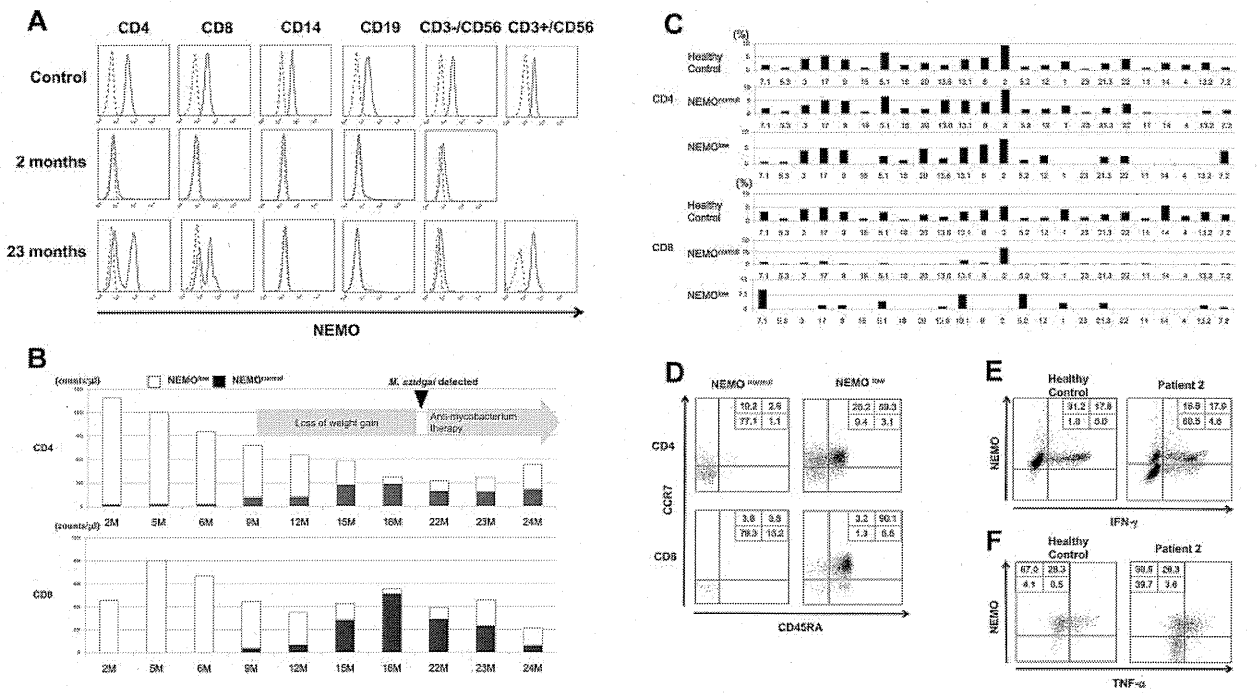

Figure 1. Identification and characterization of *NEMO* revertant T cells in patient 2. (A) Intracellular expression of NEMO in various PBMC lineages from a healthy adult control and patient 2 were evaluated by flow cytometry. For the patient, results of the analyses performed at 2 months and 23 months are shown. Solid lines indicate staining with the anti-NEMO mAb, and dotted lines indicate the isotype control. (B) Time-course variations in the absolute count of $NEMO^{normal}$ and $NEMO^{low}$ T cells in patient 2. M indicates age in months. (C) TCR-Vβ repertoire analysis of the patient's $CD4^+$ and $CD8^+$ T cells. PBMCs from the patient and a healthy adult control were stained for the TCR-Vβ panel, CD4, CD8, and NEMO, and analyzed by flow cytometry. (D) Phenotype analysis of T cells in patient 2. PBMCs from the patient and a control were stained for the expression of NEMO, CCR7, CD45RA, and CD4 or CD8. Data shown were gated on $NEMO^{normal}$ or $NEMO^{low}$ $CD4^+$ or $CD8^+$ cells. (E-F) Cytokine production from $NEMO^{normal}$ and $NEMO^{low}$ T cells. PBMCs from the patient and a control were stimulated with PMA and ionomycin for 6 hours and stained for intracellular (E) IFN-γ or (F) TNF-α along with NEMO. Cells shown are gated on the $CD3^+$ population.

because of X-chromosome inactivation. This analysis assumes that the percentage of cDNA for wild-type *NEMO* reflects the percentage of cells expressing wild-type NEMO. A high proportion of wild-type *NEMO* cDNA was observed in T cells from the mothers of patients 1/2, 3, 8, and 10, although wild-type *NEMO* cDNA was not predominant in T cells from the mother of patient 4 (Table 5).

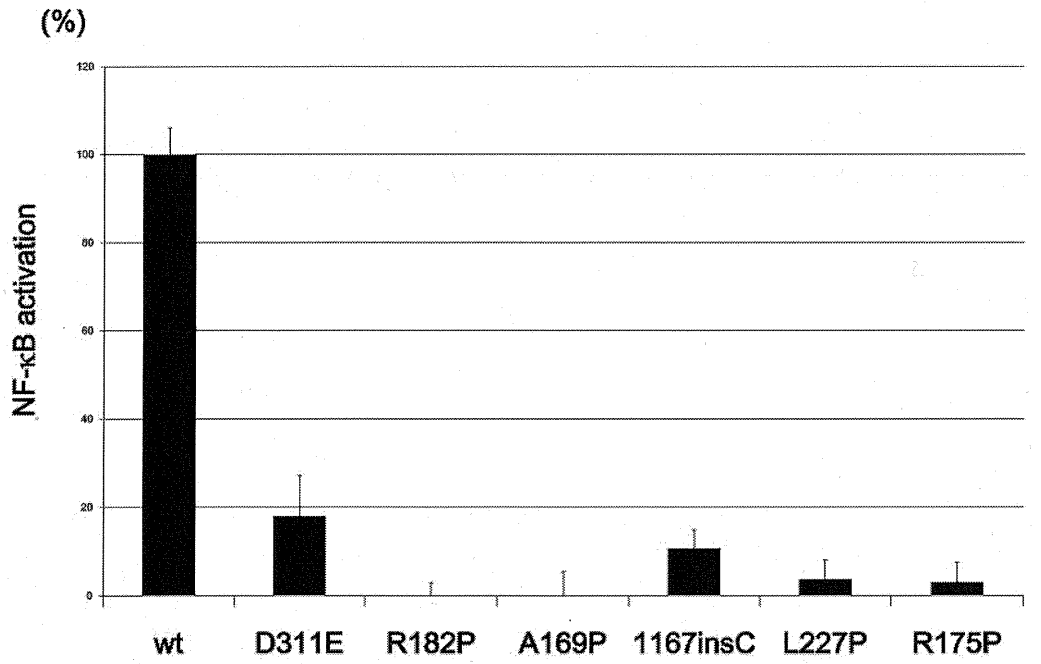

Figure 2. NF-κB transactivation by NEMO mutants from the XL-EDA-ID patients. NF-κB transactivation induced by NEMO mutants in the XL-EDA-ID patients. Mock vectors and wild-type (wt) NEMO were used as controls. The NF-κB activation index of NEMO variants were calculated as (NF-κB activation by each NEMO variant − NF-κB activation of the mock vector)/(NF-κB activation by wild-type NEMO − NF-κB activation of the mock vector). The data shown are the mean ± SD of triplicate wells and are representative of 3 independent experiments with similar results.

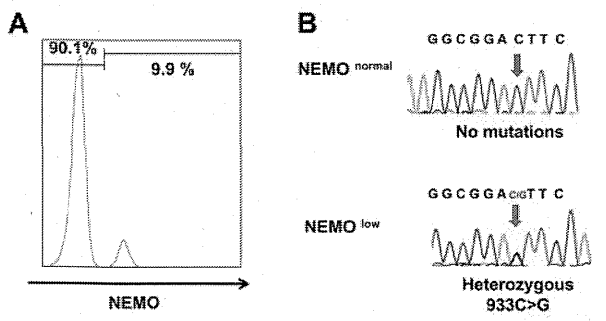

Figure 3. *NEMO* revertant T cells in patient 3. (A) Intracellular expression of NEMO in $CD8^+$ cells from patient 3. (B) Sequencing chromatograms of DNA from $NEMO^{normal}$ or $NEMO^{low}$ $CD8^+$ cells of patient 3. Arrows indicate the mutated base position at c. 931.

Similarly, there was an apparent high proportion of wild-type *NEMO* cDNA in monocytes and B cells from the mothers of patients 1/2, 8, and 10 (Table 5). These findings suggested a general selective advantage of $NEMO^{normal}$ cells over $NEMO^{low}$ cells in vivo, especially in T cells.

Proliferation capacity of $NEMO^{normal}$ and $NEMO^{low}$ T cells

T-cell proliferation stimulated by mitogens such as PHA is usually not reduced in XL-EDA-ID patients. However, the emergence of $NEMO^{normal}$ cells coincided with a reduction in mitogen-induced proliferation in patient 2. To further determine the effect of $NEMO^{normal}$ cells on mitogen-induced proliferation of peripheral T cells, the proportions of T cells carrying the wild-type and mutant were examined before and after PHA stimulation in XL-EDA-ID patients and their mothers (Table 6). In patients 2, 4, and 8, the percentage of the $NEMO^{normal}$ cells decreased after PHA stimulation, while $NEMO^{normal}$ cells prevailed in patient 9. In the mothers of patient 4 and 10, the percentage of $NEMO^{normal}$ cells increased after PHA stimulation, while the percentage of the $NEMO^{normal}$ cells decreased in the mother of patient 3. These results indicated that the NEMO mutation does not directly affect the mitogen-induced proliferation capacity of T cells and factors other than the *NEMO* genotype determine the proliferation capacity of $NEMO^{normal}$ and $NEMO^{low}$ T cells.

Discussion

Somatic reversion mosaicism has been described in several disorders affecting the hematopoietic system, the liver, and the skin.[23,26] Reports of somatic reversion cases have been particularly abundant in patients with immunodeficiency diseases, including Wiskott-Aldrich syndrome (WAS)[27] and SCID, which occur because of mutations in the interleukin receptor common γ chain,[28] CD3ζ,[29] *RAG-1*[30], and *ADA* genes.[31] Patients with somatic reversion mosaicism may present with significantly milder clinical phenotypes compared with nonrevertant patients with the same germline mutation, although this is not always the case.[26] One common feature in most cases where the somatic reversion mosaicism has been observed is a strong in vivo selective advantage of the revertant cells that express the wild-type gene product. One of the most intensively investigated diseases associated with somatic reversion mosaicism is WAS.[32-34] A report showed that up to 11% of WAS patients have presented with somatic reversion mosaicism.[33]

In our investigation, 9 of 10 XL-EDA-ID patients presented with somatic mosaicism. Two of the 9 were cases of reversion from a duplication mutation, while the others exhibited true back-reversion from a substitution or insertion mutation. This finding calls for caution when diagnosing XL-EDA-ID patients. Because the existence of a *NEMO* pseudogene makes it difficult to perform genetic analysis using genomic DNA, diagnosis of the disease is often confirmed by sequencing analysis of *NEMO* cDNA, and the presence of somatic mosaicism can cause misdiagnosis of XL-EDA-ID patients either when $NEMO^{normal}$ cells make up the majority of the patients' PBMCs or when the cDNA of the mutated *NEMO* gene cannot be amplified by PCR.[17] In fact, mutated *NEMO* cDNA could not be amplified from the PBMCs of patient 2 even when $NEMO^{normal}$ cells were absent (during early infancy), and only wild-type *NEMO* cDNA was amplified after the appearance of $NEMO^{normal}$ cells (data not shown), probably because of the instability of the mutated *NEMO* mRNA. Flow cytometric analysis of intracellular NEMO protein is of help in identifying the $NEMO^{low}$ cells in some patients, but the technique is not applicable when the *NEMO* mutation does not cause reduced expression of NEMO protein. Thus, some cases of XL-EDA-ID patients with reversion may be difficult to diagnose.

The high frequency of somatic mosaicism observed in XL-EDA-ID patients indicates a strong in vivo selective advantage for $NEMO^{normal}$ cells, which express the wild-type gene product. Patient 2 presented with a high mutant T-cell count at birth that gradually decreased over time (Figure 1B). This finding indicates that wild-type NEMO expression is critical for the survival of certain cell lineages, including T cells, after birth. On the other hand, no $NEMO^{normal}$ monocytes and very few $NEMO^{normal}$ B cells were detected in the recruited XL-EDA-ID patients (Table 4). This specific feature is similar to other somatic reversion mosaicism seen in primary immunodeficiency patients[26] and indicates that the expression of NEMO is less critical for the survival of monocytes or B cells compared with that of T cells. There is also an apparent

Table 4. Analysis of *NEMO* gene mosaicism in various cell lineages for each patient

Patient	Mutation	Age at analysis	CD4, % (proportion)	CD8, % (proportion)	CD14, % (proportion)	CD19, % (proportion)
1	Duplication	2 y	90	100	0	4.0
2	Duplication	15 mo	45	66	0	4.0
3	D311E	3 y	2.4	9.9	0	1.2
4	A169P	12 y	0 (0/19)	24 (9/37)	0 (0/19)	0 (0/47)
5	L227P	3 y	0 (0/25)	0 (0/35)	0 (0/30)	0 (0/25)
6	R182P	4 y	18 (5/28)	17 (9/52)	0 (0/27)	0 (0/33)
7	R175P	6 y	0.4 (1/25)	39 (11/28)	0 (0/28)	0 (0/25)
8	Q348X	8 y	38 (6/16)	47 (9/19)	0 (0/33)	0 (0/25)
9	R175P	15 y	30 (9/30)	36 (12/33)	0 (0/23)	0 (0/14)
10	1167 ins C	9 mo	PBMC 9.3 (4/43)			

For patients 1 to 3, data represent the percentages of $NEMO^{normal}$ cells in each lineage, as assessed by flow cytometry. For patients 4 to 10, the ratio indicates the number of wild-type NEMO clones in various cell lineages as compared with the total number of clones analyzed, based on subcloning and sequencing analysis.

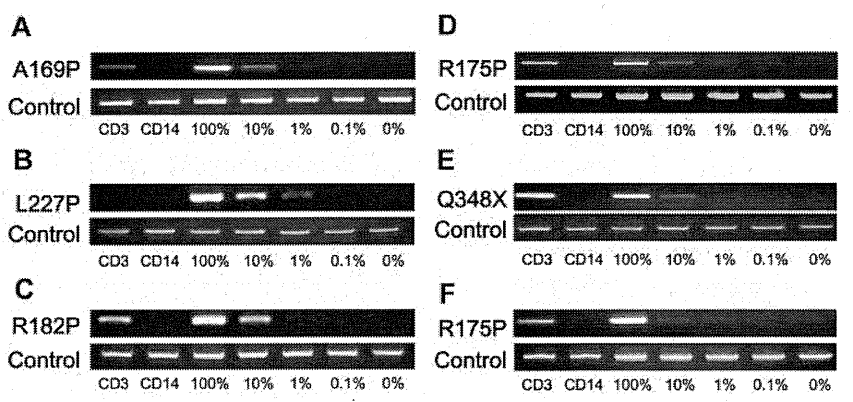

Figure 4. NEMO reversion selectively occurs in T cells of XL-EDA-ID patients. Allele-specific PCR for *NEMO* on $CD3^+$ or $CD14^+$ cells from (A) patient 4, (B) patient 5, (C) patient 6, (D) patient 7, (E) patient 8, and (F) patient 9. Numbers below each figure indicate the percentages of wild-type NEMO cDNA mixed with each mutant. Primers used in each PCR are shown on the left.

concordance between the degree of the disruption of *NEMO* gene and the proportion of reverted $NEMO^{normal}$ cells compared with $NEMO^{low}$ cells. The high proportion of reverted T cells seen in patients 1 and 2 as well as in patient 8 was associated with a highly disruptive mutation of the *NEMO* gene (ie, a duplication mutation in patients 1 and 2, and a truncation mutation in patient 8). In addition, the highly selective X-chromosome inactivation observed in the mothers of XL-EDA-ID patients indicated a strong selective advantage for $NEMO^{normal}$ cells over $NEMO^{low}$ cells. It is also noteworthy that reverted T cells were not detected in patient 5, who carried an L227P mutation that was not localized to either of the functional domains in the NEMO protein. Other reported cases with the same mutation presented with polysaccharide-specific humoral immunodeficiency and autoinflammatory diseases, but were spared complications such as cellular immunodeficiency and susceptibility to *Mycobacterium* (similar to patient 5).[4,8] This may reflect the fact that the L227P mutation in NEMO has less influence on T-cell growth than NEMO mutations that occur in functional domains, and suggests that reversion of the mutation has little impact on T-cell survival. Although the number of cases in our study is limited, it appears that the more disruptive NEMO mutations favor the survival of $NEMO^{normal}$ cells after reversion and X-chromosome inactivation.

Regarding the gradual decline in the number of NEMO-deficient T cells, one candidate trigger could be infection. Because the dominance of the memory phenotype and the skewed TCR repertoire among $CD8^+$ T cells in $NEMO^{normal}$ cells were observed in both patients 1 and 2 (Figure 1C and Mizukami et al[18]), continuous infection of pyogenic bacteria in patient 1 and *M szulgai* in patient 2 could be a reason for the emergence of $NEMO^{normal}$ cells and the elimination of $NEMO^{low}$ cells. The decrease in $NEMO^{normal}$ cells and restoration of $NEMO^{low}$ cells after anti-mycobacterial therapy in patient 2 support this hypothesis. In the case of patient 1, the predominance of $NEMO^{normal}$ T cells with an effector/memory phenotype at diagnosis (Table 4 and Mizukami et al[18]) is likely to be the result of chronic infection, and it is possible that $NEMO^{low}$ cells were predominant during his early infancy. Because some reports have indicated that TNF-α–induced programmed cell death of several cell types, including a human T-cell line, was enhanced by hypomorphic *NEMO* mutations,[12,35] and considering our finding that the levels of TNF-α expressed in revertant T cells were similar to levels in healthy control T cells in vitro (Figure 1F), TNF-α produced from these cells in response to infection could be involved in mutant T-cell elimination.

Unexpectedly, T-cell proliferation in patient 2 was equivalent to that of normal controls at the age of 2 months and was reduced after $NEMO^{normal}$ T cells increased (Figure 1B; Table 3). This finding indicates that the $NEMO^{low}$ T cells did not have intrinsically impaired mitogen-induced proliferation. One reasonable explanation for the reduced proliferation observed after the increase in $NEMO^{normal}$ T cells is a reduction in the absolute number of T cells (naive T cells in particular), probably because of the infection.

Table 5. Expression of mutant NEMO in various cell lineages for the mother of each XL-EDA-ID patient

Sample	Mutation	Analysis	Subtype	Mutant type, % (proportion)
Mother of patients 1 and 2	Duplication	FACS	CD3	0
			CD14	0
			CD19	0
Mother of patient 3	D311E	FACS	CD3	13
			$CD3^-$	54
		Subcloning	CD3	22 (6/27)
			$CD3^-$	55 (12/22)
Mother of patient 4	A169P	Subcloning	CD3	52 (11/21)
			CD14	58 (11/19)
			CD19	42 (5/12)
Mother of patient 8	Q348X	Subcloning	CD3	0 (0/26)
			CD14	17 (3/18)
			CD19	0 (0/18)
Mother of patient 10	1167insC	Subcloning	CD3	18 (7/39)
			CD14	12 (5/43)
			CD19	27 (12/44)

Data are shown as either the percentages of $NEMO^{normal}$ cells, as assessed by flow cytometry, or as the ratio of clones containing wild-type NEMO to the total number of clones, as analyzed by subcloning and sequencing analysis.

Table 6. Expression of mutant NEMO in CD3-positive cells and PHA blasts

Sample	Mutations	Analysis	Subtype	Mutant type, % (proportion)
Mother of patient 3	D311E	FACS	CD3	13
			PHA blast	47
		Subcloning	CD3	22 (6/27)
			PHA blast	48 (11/23)
Mother of patient 4	A169P	Subcloning	CD3	52 (11/21)
			PHA blast	18 (9/49)
Mother of patient 8	Q348X	Subcloning	CD3	0 (0/26)
			PHA blast	0 (0/21)
Mother of patient 10	1167insC	Subcloning	CD3	18 (7/39)
			PHA blast	9 (4/43)
Patient 2	Duplication	FACS	CD3	73
			PHA blast	93
Patient 4	A169P	Subcloning	CD3	79 (19/24)
			PHA blast	100 (37/37)
Patient 8	Q348X	Subcloning	CD3	56 (18/32)
			PHA blast	100 (16/16)
Patient 9	R175P	Subcloning	CD3	87 (34/39)
			PHA blast	0 (0/28)

PHA blasts were obtained by incubating PBMCs with PHA and soluble IL-2 for 7 days. Data are shown as either the percentages of $NEMO^{normal}$ cells, as assessed by flow cytometry, or as the ratio of clones containing wild-type NEMO to the total number of clones, as analyzed by subcloning and sequencing analysis.

Therefore, to identify other mechanisms underlying reduced T-cell proliferation, the impact of *NEMO* mutation on PHA-induced T-cell proliferation was indirectly examined in vitro by comparing the response of $NEMO^{normal}$ and $NEMO^{low}$ cells derived from XL-EDA-ID patients and their mothers. After PHA stimulation and proliferation, the proportion of $NEMO^{low}$ T cells increased in patients 2, 4, and 8, while the opposite result was observed in patient 9 and in the mother of patient 4 (Table 6). Although the precise mechanism is unclear, a reduction in the proportion of $NEMO^{normal}$ cells after PHA stimulation would reflect the lower proliferative capacity of $NEMO^{normal}$ cells compared with that of $NEMO^{low}$ cells, which may be another explanation for the reduced T-cell proliferation observed in patient 2 at 23 months of age when $NEMO^{normal}$ T cells were dominant. In the reports on reversion mosaicism of *IL2RG* gene mutations,[28,36] the restoration of T-cell function and clinical symptoms varied among patients. Therefore, other factors besides the genotype of the mutations, such as the developmental stage where reversion occurred and the frequency of reversion, affect the clinical impact of somatic mosaicism of *NEMO* gene mutations.

In this study, the effect of somatic mosaicism of the *NEMO* gene on clinical phenotype could not be fully evaluated. However, cytokines produced by revertant T cells could influence the development of clinical symptoms of XL-EDA-ID, such as inflammatory bowel disease. In a mouse model, intestinal epithelial cell-specific inhibition of NF-κB through the conditional ablation of NEMO resulted in the development of chronic bowel inflammation sensitized intestinal epithelial cells to TNF-α–induced apoptosis.[37] In this model, the first phase of intestinal inflammation was initiated by epithelial cell death and was followed by a second phase of TNF-α–induced intestinal inflammation, the latter being dependent on T cells. Another report showed that HSCT in XL-EDA-ID patients exacerbated the patients' inflammatory bowel disease.[38] Indeed, in patient 4, the percentage of reverted T cells was reduced after repeated administrations of anti-TNFα blocking Ab, and the symptoms of inflammatory bowel disease improved.[18] Considering this evidence, somatic mosaicism in T cells might be an important factor leading to inflammatory disease in XL-EDA-ID patients with defective NF-κB activation. However, our study did not show a tight association between inflammatory bowel disease and somatic mosaicism, and further investigation is needed to determine whether the $NEMO^{normal}$ T cells play a role in inflammatory processes in XL-EDA-ID.

In conclusion, this study has identified a high frequency of somatic mosaicism in XL-EDA-ID patients, particularly in T cells, and has revealed important insights into human T-cell immunobiology in XL-EDA-ID. Although we could not demonstrate the clinical impact of somatic mosaicism in XL-EDA-ID patients, our findings suggest that care is required when making molecular diagnoses of XL-EDA-ID, and might shed light on the mechanisms underlying the variability in the clinical manifestation of XL-ED-ID and facilitate the search for appropriate treatments.

Acknowledgments

The authors are grateful to all the XL-EDA-ID patients and their families for their participation. They also thank Shoji Yamaoka (Department of Molecular Virology, Graduate School of Medicine, Tokyo Medical and Dental University, Tokyo, Japan) for kindly providing NEMO-null rat fibroblast cells, and Takeda Pharmaceutical Company Limited for kindly providing the recombinant human IL-2.

This work was supported by grants from the Japanese Ministry of Education, Culture, Sports, Science, and Technology, and by grants from the Japanese Ministry of Health, Labor and Welfare.

Authorship

Contribution: Tomoki Kawai wrote the manuscript and performed research; R.N., T.Y., T.N., and T.H. edited the manuscript and supervised this work; K.I., Y.M., N.T., H.S., M.S., and Y.T. cultured cells; and T. Mizukami, H.N., Y.K., A.Y., T. Murata, S.S., E.I., H.A., Toshinao Kawai, C.I., S.O., and M.K. treated patients and analyzed data.

Conflict-of-interest disclosure: The authors declare no competing financial interests.

Correspondence: Ryuta Nishikomori, MD, PhD, Department of Pediatrics, Kyoto University Graduate School of Medicine, 54 Kawahara-cho, Shogoin, Sakyo-ku, Kyoto 606-8507, Japan; e-mail: rnishiko@kuhp.kyoto-u.ac.jp.

References

1. Pinheiro M, Freire-Maia N. Ectodermal dysplasias: a clinical classification and a causal review. *Am J Med Genet.* 1994;53(2):153-162.
2. Abinun M, Spickett G, Appleton AL, Flood T, Cant AJ. Anhidrotic ectodermal dysplasia associated with specific antibody deficiency. *Eur J Pediatr.* 1996;155(2):146-147.
3. Sitton JE, Reimund EL. Extramedullary hematopoiesis of the cranial dura and anhidrotic ectodermal dysplasia. *Neuropediatrics.* 1992;23(2):108-110.
4. Schweizer P, Kalhoff H, Horneff G, Wahn V, Diekmann L. [Polysaccharide specific humoral immunodeficiency in ectodermal dysplasia. Case report of a boy with two affected brothers]. *Klin Padiatr.* 1999;211(6):459-461.
5. Abinun M. Ectodermal dysplasia and immunodeficiency. *Arch Dis Child.* 1995;73(2):185.
6. Zonana J, Elder ME, Schneider LC, et al. A novel X-linked disorder of immune deficiency and hypohidrotic ectodermal dysplasia is allelic to incontinentia pigmenti and due to mutations in IKK-gamma (NEMO). *Am J Hum Genet.* 2000;67(6):1555-1562.
7. Courtois G, Smahi A, Israel A. NEMO/IKK gamma: linking NF-kappa B to human disease. *Trends Mol Med.* 2001;7(10):427-430.
8. Doffinger R, Smahi A, Bessia C, et al. X-linked anhidrotic ectodermal dysplasia with immunodeficiency is caused by impaired NF-kappaB signaling. *Nat Genet.* 2001;27(3):277-285.
9. Rothwarf DM, Zandi E, Natoli G, Karin M. IKK-gamma is an essential regulatory subunit of the IkappaB kinase complex. *Nature.* 1998;395(6699):297-300.
10. Yamaoka S, Courtois G, Bessia C, et al. Complementation cloning of NEMO, a component of the IkappaB kinase complex essential for NF-kappaB activation. *Cell.* 1998;93(7):1231-1240.
11. Smahi A, Courtois G, Vabres P, et al. Genomic rearrangement in NEMO impairs NF-kappaB activation and is a cause of incontinentia pigmenti. The International Incontinentia Pigmenti (IP) Consortium. *Nature.* 2000;405(6785):466-472.
12. Hanson EP, Monaco-Shawver L, Solt LA, et al. Hypomorphic nuclear factor-kappaB essential modulator mutation database and reconstitution system identifies phenotypic and immunologic diversity. *J Allergy Clin Immunol.* 2008;122(6):1169-1177.
13. Orange JS, Jain A, Ballas ZK, Schneider LC, Geha RS, Bonilla FA. The presentation and natural history of immunodeficiency caused by nuclear factor kappaB essential modulator mutation. *J Allergy Clin Immunol.* 2004;113(4):725-733.
14. Jain A, Ma CA, Liu S, Brown M, Cohen J, Strober W. Specific missense mutations in NEMO result in hyper-IgM syndrome with hypohydrotic ectodermal dysplasia. *Nat Immunol.* 2001;2(3):223-228.
15. Orange JS, Brodeur SR, Jain A, et al. Deficient natural killer cell cytotoxicity in patients with IKK-gamma/NEMO mutations. *J Clin Invest.* 2002;109(11):1501-1509.
16. Sebban H, Courtois G. NF-kappaB and inflammation in genetic disease. *Biochem Pharmacol.* 2006;72(9):1153-1160.
17. Nishikomori R, Akutagawa H, Maruyama K, et al. X-linked ectodermal dysplasia and immunodeficiency caused by reversion mosaicism of NEMO reveals a critical role for NEMO in human T-cell development and/or survival. *Blood.* 2004;103(12):4565-4572.
18. Mizukami T, Obara M, Nishikomori R, et al. Successful treatment with infliximab for inflammatory colitis in a patient with X-linked anhidrotic ectodermal dysplasia with immunodeficiency. *J Clin Immunol.* 2012;32(1):39-49.
19. Imamura M, Kawai T, Okada S, et al. Disseminated BCG infection mimicking metastatic nasopharyngeal carcinoma in an immunodeficient child with a novel hypomorphic NEMO mutation. *J Clin Immunol.* 2011;31(5):802-810.
20. Tono C, Takahashi Y, Terui K, et al. Correction of immunodeficiency associated with NEMO mutation by umbilical cord blood transplantation using a reduced-intensity conditioning regimen. *Bone Marrow Transplant.* 2007;39(12):801-804.
21. Saito M, Nishikomori R, Kambe N, et al. Disease-associated CIAS1 mutations induce monocyte death, revealing low-level mosaicism in mutation-negative cryopyrin-associated periodic syndrome patients. *Blood.* 2008;111(4):2132-2141.
22. Yang TP, Stout JT, Konecki DS, Patel PI, Alford RL, Caskey CT. Spontaneous reversion of novel Lesch-Nyhan mutation by HPRT gene rearrangement. *Somat Cell Mol Genet.* 1988;14(3):293-303.
23. Zhang LH, Jenssen D. Reversion of the hprt mutant clone SP5 by intrachromosomal recombination. *Carcinogenesis.* 1992;13(4):609-615.
24. Monnat RJ Jr, Chiaverotti TA, Hackmann AF, Maresh GA. Molecular structure and genetic stability of human hypoxanthine phosphoribosyltransferase (HPRT) gene duplications. *Genomics.* 1992;13(3):788-796.
25. Rautenstrauss B, Liehr T, Fuchs C, et al. Mosaicism for Charcot-Marie-Tooth disease type 1A: onset in childhood suggests somatic reversion in early developmental stages. *Int J Mol Med.* 1998;1(2):333-337.
26. Wada T, Candotti F. Somatic mosaicism in primary immune deficiencies. *Curr Opin Allergy Clin Immunol.* 2008;8(6):510-514.
27. Ariga T, Kondoh T, Yamaguchi K, et al. Spontaneous in vivo reversion of an inherited mutation in the Wiskott-Aldrich syndrome. *J Immunol.* 2001;166(8):5245-5249.
28. Stephan V, Wahn V, Le Deist F, et al. Atypical X-linked severe combined immunodeficiency due to possible spontaneous reversion of the genetic defect in T cells. *N Engl J Med.* 1996;335(21):1563-1567.
29. Rieux-Laucat F, Hivroz C, Lim A, et al. Inherited and somatic CD3zeta mutations in a patient with T-cell deficiency. *N Engl J Med.* 2006;354(18):1913-1921.
30. Wada T, Toma T, Okamoto H, et al. Oligoclonal expansion of T lymphocytes with multiple second-site mutations leads to Omenn syndrome in a patient with RAG1-deficient severe combined immunodeficiency. *Blood.* 2005;106(6):2099-2101.
31. Hirschhorn R. In vivo reversion to normal of inherited mutations in humans. *J Med Genet.* 2003;40(10):721-728.
32. Wada T, Schurman SH, Jagadeesh GJ, Garabedian EK, Nelson DL, Candotti F. Multiple patients with revertant mosaicism in a single Wiskott-Aldrich syndrome family. *Blood.* 2004;104(5):1270-1272.
33. Stewart DM, Candotti F, Nelson DL. The phenomenon of spontaneous genetic reversions in the Wiskott-Aldrich syndrome: a report of the workshop of the ESID Genetics Working Party at the XIIth Meeting of the European Society for Immunodeficiencies (ESID). Budapest, Hungary October 4-7, 2006. *J Clin Immunol.* 2007;27(6):634-639.
34. Davis BR, Yan Q, Bui JH, et al. Somatic mosaicism in the Wiskott-Aldrich syndrome: molecular and functional characterization of genotypic revertants. *Clin Immunol.* 2010;135(1):72-83.
35. Yamaoka S, Inoue H, Sakurai M, et al. Constitutive activation of NF-kappa B is essential for transformation of rat fibroblasts by the human T-cell leukemia virus type I Tax protein. *EMBO J.* 1996;15(4):873-887.
36. Speckmann C, Pannicke U, Wiech E, et al. Clinical and immunologic consequences of a somatic reversion in a patient with X-linked severe combined immunodeficiency. *Blood.* 2008;112(10):4090-4097.
37. Nenci A, Becker C, Wullaert A, et al. Epithelial NEMO links innate immunity to chronic intestinal inflammation. *Nature.* 2007;446(7135):557-561.
38. Fish JD, Duerst RE, Gelfand EW, Orange JS, Bunin N. Challenges in the use of allogeneic hematopoietic SCT for ectodermal dysplasia with immune deficiency. *Bone Marrow Transplant.* 2009;43(3):217-221.

bjh research paper

Identification of the integrin β3 L718P mutation in a pedigree with autosomal dominant thrombocytopenia with anisocytosis

Yoshiyuki Kobayashi,[1,2] Hirotaka Matsui,[1]* Akinori Kanai,[1] Miyuki Tsumura,[2] Satoshi Okada,[2] Mizuka Miki,[2] Kazuhiro Nakamura,[2] Shinji Kunishima,[3] Toshiya Inaba[1] and Masao Kobayashi[2]

[1]Department of Molecular Oncology and Leukaemia Programme Project, Research Institute for Radiation Biology and Medicine, Hiroshima University, [2]Department of Paediatrics, Graduate School of Biomedical and Health Sciences, Hiroshima University, Minami-ku, Hiroshima, and [3]Department of Advanced Diagnosis, Clinical Research Centre, National Hospital Organization Nagoya Medical Centre, Nagoya, Aichi, Japan

Received 29 June 2012; accepted for publication 22 October 2012

Correspondence: Hirotaka Matsui, Department of Molecular Oncology and Leukemia Program Project, Research Institute for Radiation Biology and Medicine, Hiroshima University, 1-2-3 Kasumi, Minami-ku, Hiroshima 734-8553, Japan.
E-mail: hmatsui@hiroshima-u.ac.jp

Summary

αIIbβ3 integrin mutations that result in the complete loss of expression of this molecule on the platelet surface cause Glanzmann thrombasthenia. This is usually autosomal recessive, while other mutations are known to cause dominantly inherited macrothrombocytopenia (although such cases are rare). Here, we report a 4-generation pedigree including 10 individuals affected by dominantly inherited thrombocytopenia with anisocytosis. Six individuals, whose detailed clinical and laboratory data were available, carried a non-synonymous *ITGB3* gene alteration resulting in mutated integrin β3 (ITGB3)-L718P. This mutation causes partial activation of the αIIbβ3 complex, which promotes the generation of abnormal pro-platelet-like protrusions through downregulating RhoA (RHOA) activity in transfected Chinese Hamster Ovary cells. These findings suggest a model whereby the integrin β3-L718P mutation contributes to thrombocytopenia through gain-of-function mechanisms.

Keywords: integrin β3 L718P mutation, familial thrombocytopenia, autosomal dominant inheritance, whole exome sequencing, inhibition of RhoA.

Lifelong haemorrhagic syndromes are in part caused by point mutations in the *ITGA2B* and *ITGB3* genes encoding ITGA2B and ITGB3 proteins (integrin αIIb and β3, respectively). The αIIbβ3 complex regulates thrombopoiesis by megakaryocytes and aggregation of platelets in response to extracellular stimuli, such as ADP and collagen. The autosomal recessive syndrome, Glanzmann thrombasthenia, is the most frequently encountered disease caused by αIIbβ3 mutations (George *et al*, 1990; Nurden, 2006; Nurden & Nurden, 2008; Nurden *et al*, 2011a). Patients have a homozygous or a compound heterozygous mutation in the *ITGA2B* or *ITGB3* genes that causes loss of function of the αIIbβ3 complex. Although platelet counts and size are generally normal, patients typically have severe mucocutaneous bleeding, such as epistaxis, menorrhagia and gastrointestinal bleeding, frequently because of defects in platelet aggregation.

Mutations of the αIIbβ3 complex are also involved in congenital haemorrhagic diseases other than Glanzmann thrombasthenia (Ghevaert *et al*, 2008; Schaffner-Reckinger *et al*, 2009; Jayo *et al*, 2010; Kunishima *et al*, 2011; Nurden *et al*, 2011b). For example, the integrin β3 D723H mutation is found in autosomal dominant macrothrombocytopenia (Ghevaert *et al*, 2008). Biochemical analysis revealed that integrin β3-D723H is a gain of function mutation which activates the αIIbβ3 complex constitutively, albeit only partially. This results in the formation of proplatelet-like protrusions in transfected Chinese Hamster Ovary (CHO) cells, a model of relevance for the formation of macrothrombocytes (Ghevaert *et al*, 2008; Schaffner-Reckinger *et al*, 2009).

More recently, a sporadic patient carrying an integrin β3-L718P mutation was reported (Jayo *et al*, 2010). She had mild thrombocytopenia (127×10^9/l), platelet anisocytosis and reduced platelet aggregation potential. This mutation also induces abnormal proplatelet formation.

In the present study, we report a pedigree with a total 10 of individuals affected by a dominantly inherited haemorrhagic

First published online 17 December 2012
doi:10.1111/bjh.12160

syndrome. Six individuals whose detailed clinical and laboratory data are available, presented with thrombocytopenia accompanied by anisocytosis and carry a non-synonymous *ITGB3* T2231C alteration resulting in the integrin β3-L718P mutation. We also performed entire exon sequencing by a next-generation sequencing and found that the integrin β3-L718P mutation is most likely the sole gene responsible for thrombocytopenia in this pedigree.

Materials and methods

Written informed consent was obtained from individuals in the family in accordance with the Declaration of Helsinki for blood sampling and analysis undertaken with the approval of the Hiroshima University Institutional Review Board.

Patient

The patient was 4-year-old Japanese girl (iv.3 in Fig 1A), who presented with mild bleeding tendencies, such as recurrent nasal bleeding and purpura in her extremities. Her platelet count was 49–72 × 10^9/l with a mean platelet volume (MPV) of 9·8–10·9 fl. White blood cell and red blood cell counts were within the normal range and there were no morphological abnormalities including inclusions in neutrophils. Bone marrow examination was not performed. A total of six of her relatives, namely her father (iii.2), sister and brother (iv.1 and iv.2), two cousins (iv.4 and iv.5) and an aunt (iii.5), were subsequently found to have low platelet counts and were referred to our institute for further investigation.

Antibodies and reagents

Unconjugated or phycoerythrin-cyanin 5 (PC5)-conjugated anti-CD41 monoclonal antibody (Ab) (clone P2) against the αIIbβ3 complex (Beckman Coulter, Brea, CA, USA), fluorescein isothiocyanate (FITC)-conjugated anti-CD41a monoclonal Ab (clone HIP8) (Beckman Coulter), FITC- or peridinin chlorophyll (PerCP)-conjugated anti-CD61 monoclonal Ab (clone RUU-PL 7F12) (BD Biosciences, San Jose, CA, USA), FITC-conjugated PAC-1 (BD Biosciences) and Alexa488-conjugated human fibrinogen (Life Technologies, Carlsbad, CA, USA) were used in flow cytometry. Anti-CD61 monoclonal Ab (clone EP2417Y) (Abcam, Cambridge, UK), anti-DDDDK-tag polyclonal Ab (Medical & Biological Laboratories, Nagoya, Japan), Alexa488-conjugated phalloidin and Hoechst 33342 (both Life Technologies) were used for immunofluorescence microscopy. The oligopeptide Arg-Gly-Asp-Ser (RGDS) (Sigma–Aldrich, St Louis, MO, USA) was used to competitively inhibit the binding of ligands to αIIbβ3, and adenosine diphosphate (ADP) (nacalai tesque, Kyoto, Japan) was used for the stimulation of αIIbβ3 on platelets.

Construction and transfection of expression vectors

Full-length wild type (WT) *ITGA2B* and *ITGB3* cDNA were amplified by polymerase chain reaction (PCR) and cloned into pcDNA3·1 expression vectors. A PCR-mediated site-directed mutagenesis technique was applied to produce *ITGB3* mutants encoding integrin β3-L718P, -D723H and -T562N with or without truncation at the C-terminal side of Y^{759} (del. 759). *RHOA* cDNA, which encodes RhoA (RHOA) protein, was amplified by PCR and its mutants (T19N and Q63L) were generated by site-directed mutagenesis, followed by cloning into p3xFLAG-CMV-10 vectors (Sigma–Aldrich). The *ITGA2B* and *ITGB3* expression vectors were simultaneously transfected into CHO cells cultured in Ham's F12 medium supplemented with 10% fetal bovine serum at 37°C, in 5% CO_2, using Lipofectamine LTX reagent (Life Technologies) according to the manufacturer's instructions.

Immunofluorescent laser-scanning confocal microscopy

Cells grown on coverslips coated with 100 μg/ml fibrinogen were fixed with 4% paraformaldehyde, followed by permeabilization with phosphate-buffered saline containing 0·1% Triton X100. After blocking, the cells were stained with primary antibodies at appropriate dilutions, followed by staining with Alexa488- or Cy3-conjugated secondary antibodies together with Hoechst 33342. High-resolution immunofluorescent images were taken under a laser-scanning confocal microscopy (LSM5 Pascal, Carl Zeiss, Oberkochen, Germany) using a x63 objective.

Flow cytometry

The expression and activation of integrin αIIb and β3 on the platelet surface was indirectly estimated by flow cytometry with the antibodies described above. Mean fluorescence intensity (MFI) of values in an affected individual were divided by those in an unrelated normal control and recorded as relative MFI value (%). For the quantitative determination of αIIbβ3 molecules on the platelet surface, QIFIKIT (Dako, Glostrup, Denmark) was used according to the manufacturer's instructions. MFI of the calibration beads containing five populations (antibody-binding capacity: 2600, 9900, 46 000, 221 000 and 741 000) were 16·12, 63·83, 262·84, 1483·2 and 3772·1, respectively, whereas that of the negative control sample was 1·62. Therefore, αIIbβ3 molecules (copies/platelet) was calculated as $10^{(1.022 \times \log(\mathrm{MFI}) + 2.1679)} - 241$. Activation of platelets and CHO cells was estimated by methods previously described (Shattil *et al*, 1987; Hughes *et al*, 1996). Activation index was defined as $(F-F_0) / (F'-F_0)$, where F is the MFI of PAC-1-stained CHO cells transfected with αIIbβ3-L718P or αIIbβ3-D723H, and F_0 and F' are those transfected with αIIbβ3-WT and αIIbβ3-T562N, respectively. The samples were analyzed on a FACS Calibur (Becton Dickinson, Franklin Lakes, NJ, USA), equipped with an argon laser operating at 488 nm.

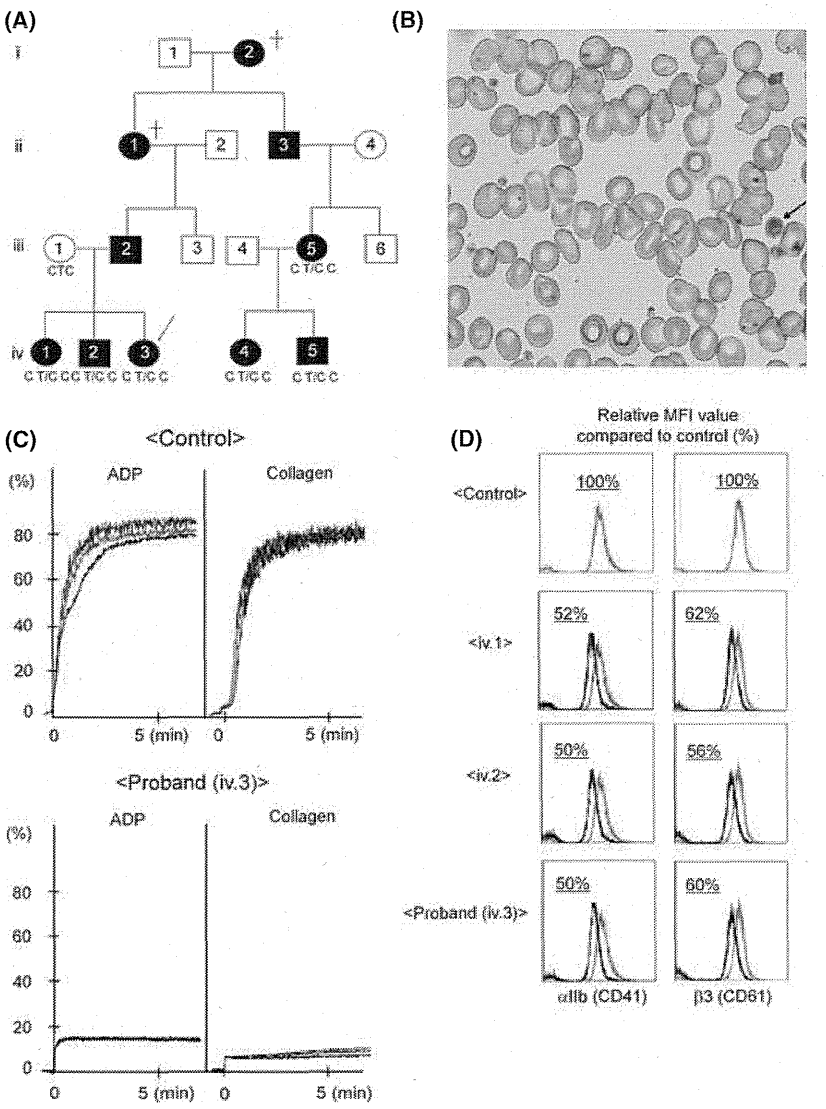

Fig 1. Platelet morphology and aggregation tracings. (A) The pedigree shows affected (filled) and unaffected (open) females (circles) and males (squares). The patient is indicated by an arrow. (B) Platelet morphology as determined by optical microscopy. Peripheral blood specimen obtained from the patient stained with May-Giemsa. The arrow indicates a macrothrombocyte. Original magnification × 600. (C) Representative platelet aggregation tracings in response to ADP and collagen stimuli in platelet-rich plasma from the patient and an unrelated normal control. (D) Flow cytometry of surface integrin αIIb (CD41) and β3 (CD61) expression. Samples were obtained from three affected individuals of the pedigree and an unrelated normal control. Data were calculated as relative MFI value (%), where MFIs of affected individuals were divided by MFI of a control sample.

Exome sequencing

Genomic DNA was obtained from four affected individuals in the pedigree and whole exome sequencing was performed. Briefly, 3 μg genomic DNA was fragmented by Covaris S2 (Covaris, Woburn, MA, USA) and ligated to adaptors, followed by hybridization to biotinylated RNA baits according to the manufacturer's instruction (Agilent Technologies, Santa Clara, CA, USA). The generated sequence tags were sequenced by the 76 bp paired-end protocol of Illumina GAIIx (Illumina, San Diego, CA, USA) and mapped onto the human genomic sequence (hg18, UCSC Genome Browser) using the sequence alignment program Eland (Illumina). Unmapped or redundantly mapped sequences were removed from the data set, and only uniquely mapped sequences were used for further analyses. Positions relative to RefSeq genes were calculated based on the respective genomic coordinates. Genomic coordinates of exons and the protein-coding regions of the RefSeq transcripts are as described in hg18. To verify the presence of *ITGB3* gene alteration, amplification and direct sequencing of a part of exon 14 was performed with the following primers; 5′-CATAGCCAGTTCAAGTGACTCCTG-3′ for forward primer and 5′-ACGATGGTACTGGCTGAACATGAC-3′ for reverse primer.

Results

Pedigree of a family with autosomal dominant thrombocytopenia with anisocytosis

In the original patient, marked platelet anisocytosis was observed in peripheral blood samples (Fig 1B). Platelet aggregation induced by ADP (1–4 μmol/l) and collagen (0·5–2 μg/ml) was markedly reduced (Fig. 1C and Table I), but agglutination induced by ristocetin (1·25 mg/ml) was within

the normal range (data not shown). Three affected individuals (iii.5, iv.1, and iv.2) showed abnormalities in platelet function similar to those of the original patient. In these affected individuals, the αIIb and β3 expression levels, which were indirectly estimated as relative MFI value (%), were 43–75% of a healthy control (Fig 1D and Table I). The number of αIIbβ3 molecules on the platelet surface in patients, as evaluated by flow cytometry using QIFIKIT, was 35 000–38 400 copies/platelet (MFI: 212·1 –232·4), whereas in an unaffected individual of the pedigree (iii.1) and an unrelated control, there were 65 200 and 62 100 copies/platelet (MFI: 389·2 and 371·3), respectively (Table I). The tendency to bleed was mild to moderate, as exemplified by the following episodes: when family member iv.1 received a bruise to the face, treatment with recombinant Factor VIIa was required because of persistent epistaxis; also, family member iii.5 had had to give birth by Caesarean section because of low platelet count. The family pedigree (Fig 1A), which shows no evidence of consanguineous marriage, strongly suggests the inheritance of thrombocytopenia as an autosomal dominant trait. The laboratory findings are shown in Table I.

Identification of the integrin β3 L718P mutation by whole exome analysis

To isolate a candidate gene alteration responsible for the thrombocytopenia, whole exome sequencing analysis was performed using genomic DNA obtained from the patient (iv.3), her sister and brother (iv.1 and iv.2) and a cousin (iv.4). A total of 794 non-synonymous gene alterations among 1551 SNPs that are not registered in dbSNP 129/130 were detected in the patient. To isolate the responsible gene, we selected non-synonymous gene alterations shared by the four affected individuals as strong candidates. Among the 90 alterations commonly found in the affected individuals of the pedigree (individual numbers of SNPs/mutations are shown in Table II), we focused on the heterozygous non-synonymous T2231C alteration in exon 14 of the *ITGB3* gene, which results in the substitution of leucine at 718 for proline (L718P) in the integrin β3 protein. We selected this because it was recently reported as a candidate mutation responsible for thrombocytopenia (Jayo *et al*, 2010). The presence of the mutation in six affected individuals of the pedigree (iv.1, iv.2, iv.3, iv.4, iii.5 and iv.5) and its absence in an unaffected individual (iii.1) and an unrelated control was confirmed by a direct-sequencing (Fig 2). As far as we could determine, no other non-synonymous gene alterations previously reported to cause thrombocytopenia or defective platelet function were present in the affected individuals of the pedigree. In addition, the L718 residue in integrin β3 is well-conserved between species and amino acid substitution in this position is predicted by bioinformatic tools, including Polyphen and SIFT, to cause a significant change in protein structure and function (data not shown). These observations strongly suggest that the L718P mutation in integrin β3 is the responsible gene alteration that causes familial thrombocytopenia.

Constitutive but partial activation of the αIIbβ3 complex by β3-L718P

To elucidate the effects of the integrin β3-L718P mutation on the activation status of αIIbβ3 complexes in resting or ADP-activated platelets, fresh platelets were analysed by flow cytometry using PAC-1, a ligand-mimicking antibody that specifically recognizes the activated form of the αIIbβ3 complex (Shattil *et al*, 1987).

Resting control platelets from healthy individuals bound PAC-1 with a similar affinity to those treated with RGDS, a peptide which competitively inhibits the binding of ligands for

Table I. Laboratory data of seven individuals of the pedigree.

						Relative MFI value compared to control (%)		αIIbβ3	molecules	Platelet (%)	aggregation
Patient	Sex	Age (years)	Platelet count ($\times 10^9$/l)	MPV (fl)	PDW (%)	αIIb	β3	MFI	copies/platelet	ADP (4 μM)	collagen (2·0 μg/ml)
iii.1	F	37	210	10·2	12·1	110	111	389·2	65 200	NA	NA
iii.5	F	34	38–67	8·5–11·3	10·0–19·0	43	75	NA	NA	15	12
iv.1	F	11	30–43	7·8–11·2	9·7–16·3	52	62	232·4	38 400	16	8
iv.2	M	8	49–64	10·3–11·1	10·1–14·7	50	56	216·4	35 700	23	16
iv.3	F	6	49–72	9·8–10·9	11·1–13·3	50	60	212·1	35 000	12	8
iv.4	F	4	32–59	9·9–10·8	12·3–15·6	NA	NA	NA	NA	NA	NA
iv.5	M	2	28–50	8·9–9·0	18·0–18·4	49	51	NA	NA	NA	NA

MPV, mean platelet volume (normal range: 9·4–12·3 fl); PDW, platelet distribution width (normal range: 9·5–14·8 %); NA, not available.
αIIbβ3 molecules (copies/platelet) were calculated as $10^{(1\cdot022 \times \log(\mathrm{MFI}) + 2\cdot1679)} - 241$ (see *Materials and methods*).

Table II. Number of SNPs/mutations detected by whole exome sequencing.

Case	iv.1	iv.2	iv.3	iv.4
SNP	21 531	21 697	20 413	20 113
Not in dbSNP 129 and 130	1 674	1 722	1 473	1 551
Non-synonymous alternations				
Homozygous	62	58	65	42
Heterozygous	800	815	667	752
Non-synonymous (common)	90			

αIIbβ3 complex such as fibrinogen and PAC-1 (Fig 3A, compare black and blue lines), indicating that wild-type αIIbβ3 in resting platelets is not activated. In contrast, platelets obtained from the affected individuals (iii.5, iv.1, iv.2 and iv.3) showed a slight increase of PAC-1 binding compared to those treated with RGDS (Fig 3A). Indeed, resting platelets from affected individuals showed a slight but significant increase of PAC-1 binding relative to healthy individuals (Fig 3A, top panel). In addition, flow cytometric analysis using FITC-conjugated fibrinogen also showed a significant increase of fibrinogen binding potential in resting platelets from affected individuals compared with healthy controls (bottom panel). Because MPV (shown in Table I) did not exceed the normal range (9·4–12·3 fl) and surface expression levels of αIIbβ3 were lower in patients than controls (Fig 1D), it is proposed that these observations indicate spontaneous activation of αIIbβ3-L718P in resting platelets.

ADP-activated platelets from healthy volunteers, on the other hand, bound to PAC-1 with a very high affinity (Fig 3B, red lines and 3B, top panel), as expected. In contrast, only a small increase of affinity to PAC-1 was observed in ADP-treated platelets carrying the β3-L718P mutation, resulting in a marginal increase of binding potential (bottom panel). These findings suggest that αIIbβ3-L718P is partially activated in the absence of inside-out signals such as ADP, but nevertheless cannot be fully activated in the presence of such signals.

To confirm the contribution of the integrin β3-L718P mutation to spontaneous activation of αIIbβ3, CHO cells were transiently transfected with expression vectors encoding integrin β3-WT, -L718P, -D723H or -T562N together with a vector encoding αIIb-WT. Flow cytometric analysis (Fig 3C) revealed that αIIbβ3-L718P expressed in CHO cells bound to PAC-1 to the same degree as αIIbβ3-D723H, a mutant previously reported to partially activate αIIbβ3, and to a lesser extent than a fully active αIIbβ3-T562N mutant (Kashiwagi *et al*, 1999). We calculated the activation indices (see *Materials and methods*) (Hughes *et al*, 1996; Schaffner-Reckinger *et al*, 2009) of αIIbβ3-L718P and -D723H as 0·23 ± 0·07 and 0·16 ± 0·02, respectively, taking αIIbβ3-T562N as fully active (=1·0) and αIIbβ3-WT as inactive (=0) (Fig 3D). Because CHO cells were not stimulated by ADP in this experiment, each index represents αIIbβ3 activation status at rest.

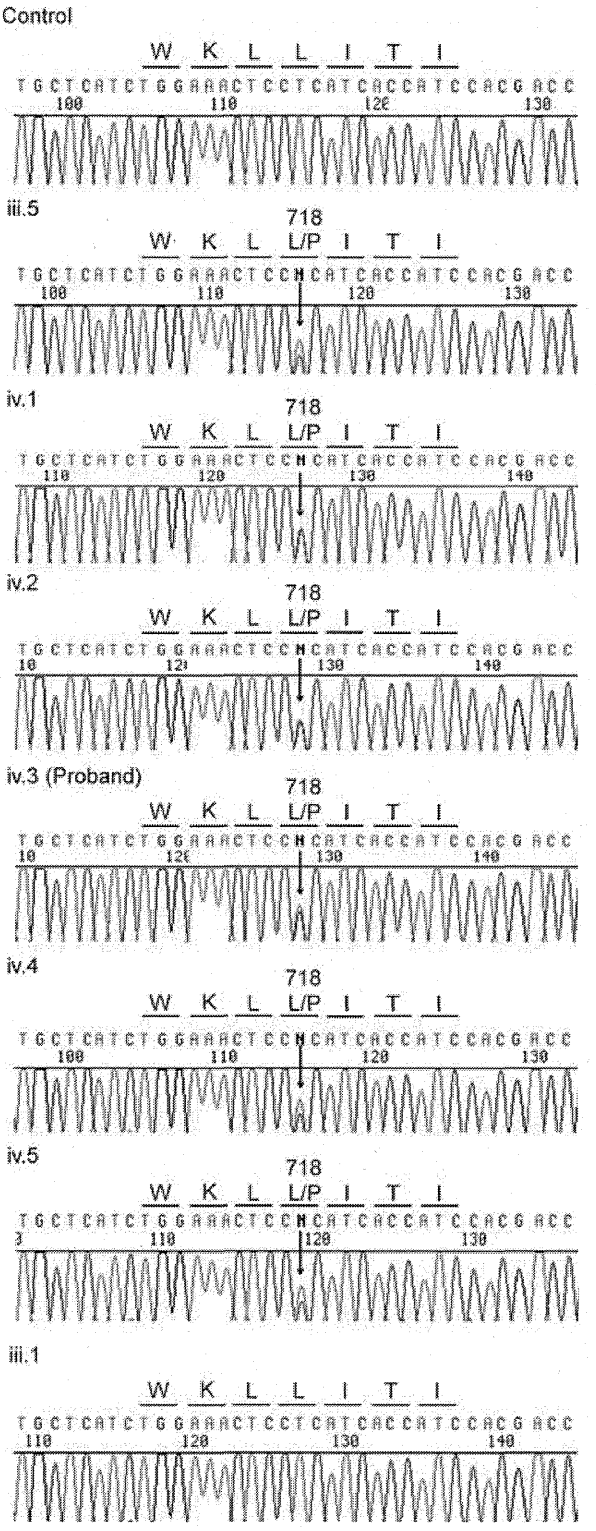

Fig 2. Direct sequencing analysis around T2231 in exon 14 of the *ITGB3* gene. Genomic DNA extracted from the affected and unaffected individuals of the pedigree were amplified by polymerase chain reaction and sequenced. Arrows indicate the position of the T2231 mutation in the *ITGB3* gene.

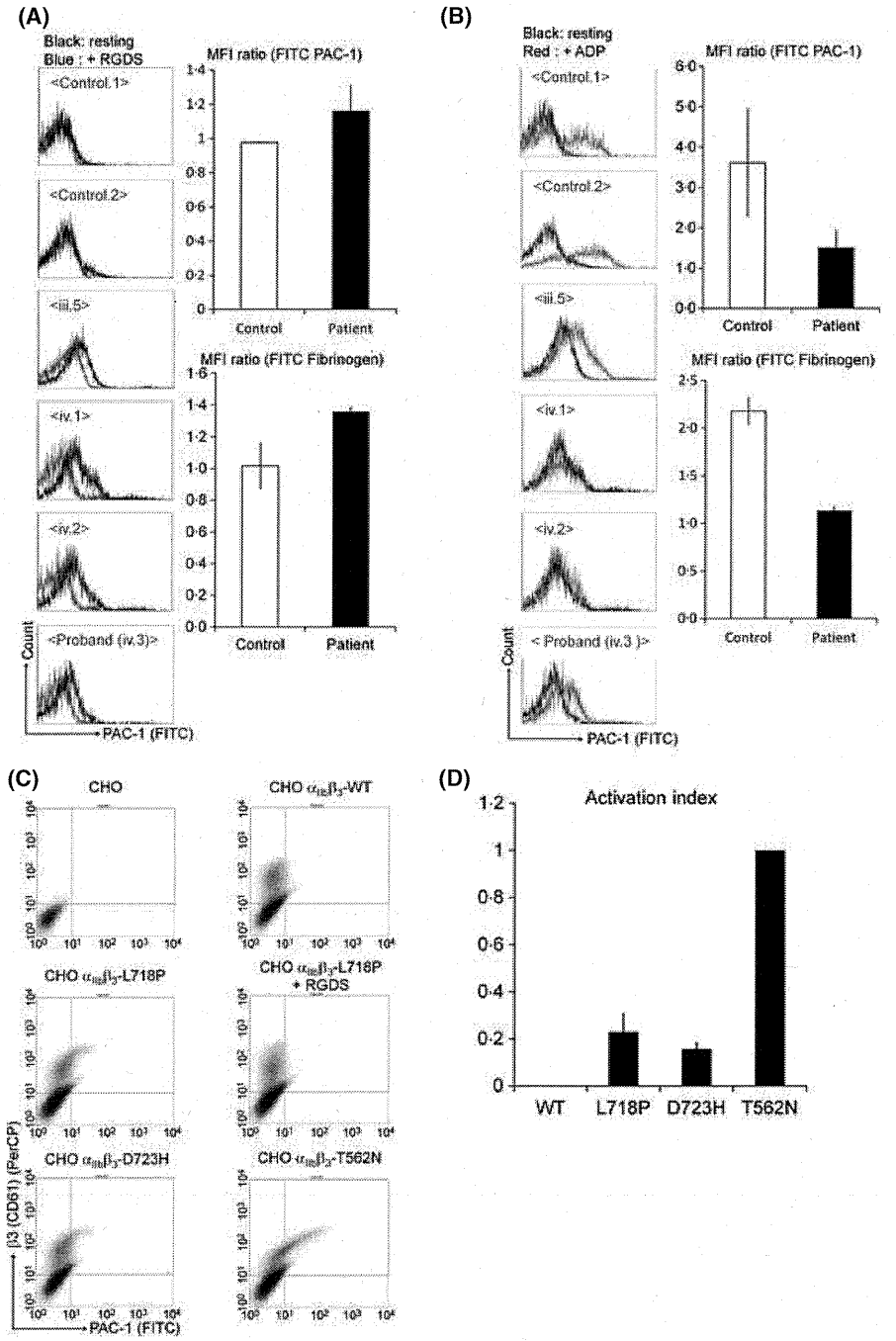

Fig 3. Functional analysis of integrin β3-L718P mutation. (A) Spontaneous binding of PAC-1 antibody to platelets obtained from affected individuals of the pedigree. Non-activated platelets (within 10 min after blood collection), incubated with or without 1 mM RGDS, were stained with FITC-conjugated PAC-1 antibody. After fixation, binding of PAC-1 to platelets was analysed by flow cytometry. Activation status of αIIbβ3 complex on resting platelets bound to FITC-PAC-1 (top) and FITC-fibrinogen (bottom). Mean fluorescence intensity (MFI) ratio was estimated by dividing the MFI of resting platelets by that of resting platelets incubated with RGDS. (B) Reduced activation of αIIbβ3 from affected individuals. The resting and ADP-stimulated platelets, stained with FITC-conjugated PAC-1 antibody were analysed by flow cytometry. Activation status of αIIbβ3 on stimulated platelets bound to FITC-PAC-1 (top) and FITC-fibrinogen (bottom). Values were estimated by dividing the MFI of platelets stimulated with ADP by those of resting platelets. (C) Partial activation of αIIbβ3-L718P and -D723H on CHO cells. CHO cells transfected with αIIbβ3 expression vectors (β3-WT, -L718P, -D723H and -T562N) were seeded on 100 μg/ml fibrinogen-coated coverslips in 6-well dishes. The cells, treated with or without RGDS, were stained with FITC-conjugated PAC-1 antibody and PerCP-conjugated anti-CD61 antibody and analysed by flow cytometry. (D) Activation index of αIIbβ3 mutants. Activation status of CHO cells expressing αIIbβ3-L718P and -D723H was compared with that of αIIbβ3-T562N as described in the "*Materials and methods*".

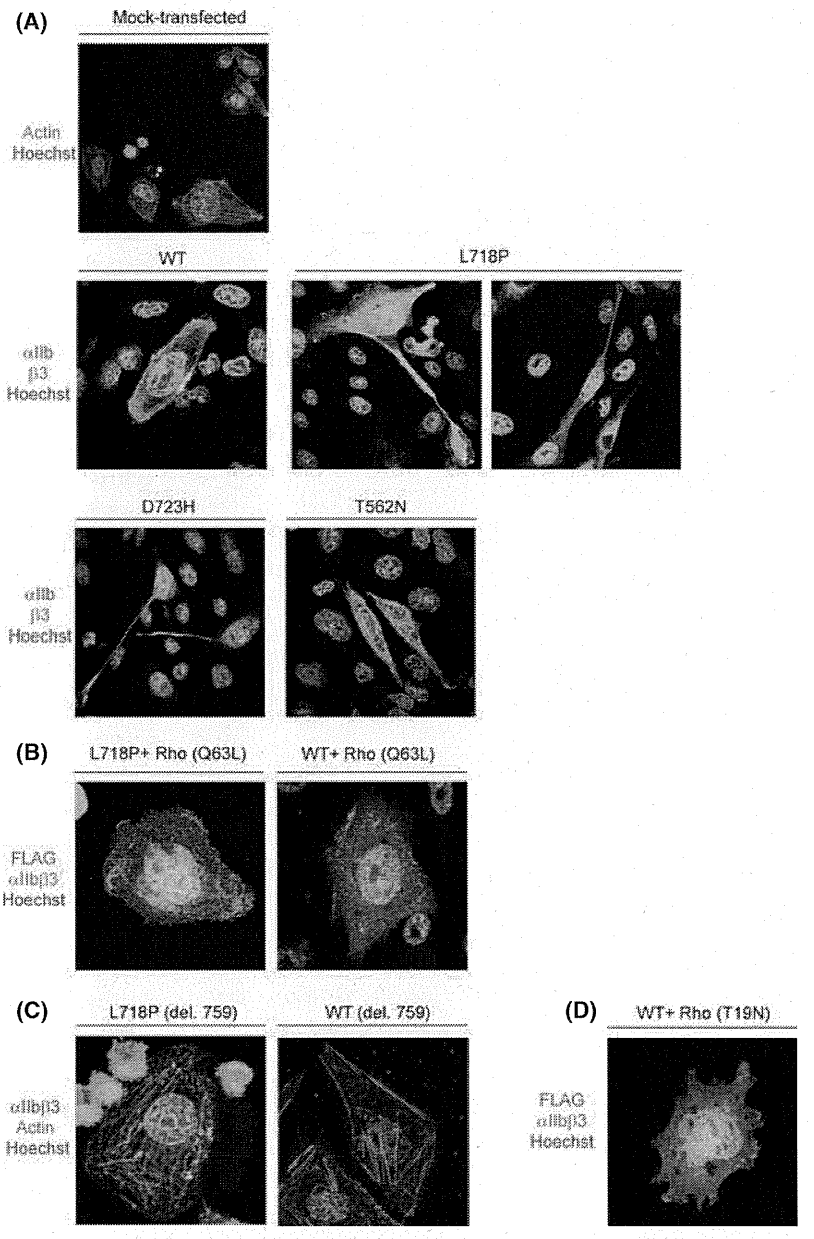

Fig 4. Overexpression of RhoA mutants or integrin β3-L718P (del. 759) modulates the formation of proplatelet-like cell protrusions in CHO cells. (A) Changes in CHO cell morphology by αIIbβ3 mutants. CHO cells transfected with αIIbβ3-L718P, -T562N and -D723H were seeded on fibrinogen-coated coverslips. After an 8-h incubation, the cells were fixed and stained with anti-CD41 and -CD61 antibodies followed by staining with Cy3- and Alexa 488-conjugated secondary antibodies. Mock-transfected cells were stained with Alexa 488-conjugated phalloidin and Hoechst 33342. (B) Inhibition of proplatelet-like protrusion formation by constitutively-active RhoA. An expression vector that encodes FLAG-tagged RhoA (Q63L) was transfected together with αIIbβ3-L718P or -WT expressing vectors into CHO cells. The cells grown on fibrinogen-coated coverslips were fixed and stained with anti-CD41 and anti-DDDDK-tag antibodies followed by staining with Alexa 488- and Cy3-conjugated secondary antibodies. (C) C-terminal deletion of β3-L718P inhibits the formation of proplatelet-like protrusions. C-terminal deleted integrin β3-L718P or -WT (del. 759) was expressed together with αIIb in CHO cells. The cells were fixed and stained with anti-CD41 antibody followed by staining with Cy3-conjugated secondary antibody and Alexa-488-labeled phalloidin. (D) A dominant-negative (T19N) form of RhoA was overexpressed in CHO cells. Images were taken as in (B).

Involvement of RhoA signalling in proplatelet-like protrusion formation

As previously reported by others (Ghevaert *et al*, 2008; Jayo *et al*, 2010), CHO cells expressing αIIbβ3-L718P, as well as αIIbβ D723H, formed long proplatelet-like protrusions on fibrinogen-coated dishes that were not observed in cells expressing wild-type αIIbβ3 (Fig 4A). In contrast, although cells expressing αIIbβ3-T562N, which yields a fully activated conformation (Kashiwagi *et al*, 1999), changed from their original round shape surrounded by a broad protrusion (Fig 4A, mock-transfected) to rhomboid-like cell morphology, proplatelet-like protrusions were rarely seen (Fig 4A). This suggests that mutants partially activating the integrin complex induce long proplatelet-like protrusions.

Recently, it was reported that the formation of proplatelet-like protrusions in CHO cells is mediated by the downregulation of RhoA activity (Chang *et al*, 2007; Schaffner-Reckinger *et al*, 2009), which is initiated by the binding of c-Src to the C-terminal tail (amino acid 760–762, Arg-Gln-Thr; RGT) of integrin β3 (Flevaris *et al*, 2007). We found that the formation of long cell protrusions was inhibited when a constitutively-active form of RhoA (Q63L) was introduced into αIIbβ3-L718P-expressing cells (Fig 4B). In addition, CHO cells expressing αIIbβ3-L718P (del. 759) mutant, which lacks the C-terminal c-Src binding site of in-

tegrin β3 (RGT), did not form any proplatelet-like protrusions (Fig 4C). Given that enforced activation of RhoA caused by introducing RhoA (Q63L), as well as de-repression of RhoA through C-terminal deletion of β3 in cells expressing αIIbβ3-WT, did not induce morphological changes in CHO cells (Figs 4B, C), it is proposed that constitutive inhibition but not activation through the c-terminal of β3 is responsible for the formation of abnormal cell protrusions in L718 mutants. However, as the enforced expression of a dominant negative form of RhoA (T19N) in αIIbβ3-WT expressing cells did not result in typical proplatelet-like protrusions (Fig 4D), this suggests that downregulation of RhoA was required but not sufficient for the formation of proplatelet-like protrusions induced by integrin β3-L718P.

Discussion

We report a pedigree with individuals suffering from a lifelong haemorrhagic syndrome, all of whom were carrying the integrin β3-L718P mutation. This had previously been reported only in a sporadic patient (Jayo *et al*, 2010). Next-generation sequencing, together with the clinical data of the patients, established that this integrin β3-L718P mutation causes thrombocytopenia resembling the disease caused by a different integrin mutation, β3-D723H, although the size of the platelets seems to differ somewhat between these mutations (Ghevaert *et al*, 2008; Schaffner-Reckinger *et al*, 2009).

Considering the dominant inheritance pattern of the haemorrhagic tendency caused by integrin β3-L718P as well as β3-D723H, these would be gain of function mutations, unlike those causing Glanzmann thrombasthenia. Indeed, expression of integrin β3-D723H partially activates the αIIbβ3 complex, resulting in downregulation of RhoA activity and induction of microtubule-dependent proplatelet-like cell protrusions considered relevant for production of macrothrombocytes (Ghevaert *et al*, 2008; Schaffner-Reckinger *et al*, 2009). Integrin β3-L718P appears to act in a similar fashion (Fig 4A and B). Interestingly, we demonstrate that the three C-terminal amino acid residues (RGT) of integrin β3 are required for L718P to form proplatelet-like cell protrusions (Fig 4C). RGT provides a binding site for c-Src tyrosine kinase, which was shown to inactivate RhoA (Flevaris *et al*, 2007), further supporting the hypothesis that integrin β3-L718P plays a role in causing megakaryocytes to produce abnormal platelets through the inhibition of RhoA.

In platelets derived from megakaryocytes that carry the integrin β3-L718P mutation, full activation of αIIbβ3 complex in response to inside-out stimuli is inhibited, as shown by reduced binding of PAC-1 and fibrinogen on stimulation with ADP (Fig 3B). A simple scenario is that, in platelets, integrin β3-L718P acts as a loss of function mutation. However, given that the carriers of Glanzmann's thrombasthenia who have both normal and mutant allele and express reduced amounts of the αIIbβ3 complex, in general show normal platelet aggregation, it is possible that the integrin β3-L718P mutation gains a function that ultimately results in the reduction of inside-out signals.

In summary, identification of a pedigree showing autosomal dominant inheritance leads to a model whereby the integrin β3-L718P mutation contributes to thrombocytopenia accompanied by anisocytosis most likely through gain-of-function mechanisms. Further investigations are necessary to fully elucidate these mechanisms by which this mutation exerts its abnormal effect on thrombocytosis and platelet aggregation.

Acknowledgements

We thank Prof. M. Matsumoto and Ms. M. Sasatani for providing clinical data; Ms. M. Nakamura, Ms. E. Kanai and Ms. R. Tai for excellent technical assistance. This work was partly supported by Grants-in-Aid for Scientific Research from the Ministry of Health, Labour and Welfare of Japan.

Author contributions

H.M., T.I. and M.K. designed the work. Y.K., H.M., A.K., S.O. and M.T. performed experiments and analysed data. S.K. contributed essential materials and interpreted data. M.M and K.N. contributed clinical materials and data. H.M, Y.K. and T.I. wrote the manuscript.

Conflict of interest

The authors declare no competing financial interests.

References

Chang, Y., Auradé, F., Larbret, F., Zhang, Y., Couedic, J.P.L., Momeux, L., Larghero, J., Bertoglio, J., Louache, F., Cramer, E., Vainchenker, W. & Debili, N. (2007) Proplatelet formation is regulated by the Rho/ROCK pathway. *Blood*, **109**, 4229–4236.

Flevaris, P., Stojanovic, A., Gong, H., Chishti, A., Welch, E. & Du, X. (2007) A molecular switch that controls cell spreading and retraction. *Journal of Cell Biology*, **179**, 553–565.

George, J.N., Caen, J.P. & Nurden, A.T. (1990) Glanzmann's thrombasthenia: the spectrum of clinical disease. *Blood*, **75**, 1383–1395.

Ghevaert, C., Salsmann, A., Watkins, N.A., Schaffner-Reckinger, E., Rankin, A., Garner, S.F., Stephans, J., Smith, G.A., Debili, N., Vainchenker, W.de, Groot, P.G., Huntington, J.A., Laffan, M., Kieffer, N. & Ouwehand, W.H. (2008) A non-synonymous SNP in the ITGB3 gene disrupts the conserved membrane-proximal cytoplasmic salt bridge in the αIIbβ3 integrin and cosegregates dominantly with abnormal proplatelet formation and macrothrombocytopenia. *Blood*, **111**, 3407–3414.

Hughes, P.E., Diaz-Gonzalez, F., Leong, L., Wu, C., McDonald, J.A., Shattil, S.J. & Ginsberg, M. H. (1996) Breaking the integrin hinge. A defined structural constraint regulates integrin signaling. *Journal of Biological Chemistry*, **271**, 6571–6574.

Jayo, A., Conde, I., Lastres, P., Martinez, C., Rivera, J., Vicente, V. & Manchón, C.G. (2010) L718P mutation in the membrane-proximal

cytoplasmic tail of β3 promotes abnormal αIIbβ3 clustering and lipid domain coalescence, and associates with a thrombasthenia-like phenotype. *Haematologica*, **95**, 1158–1166.

Kashiwagi, H., Tomiyama, Y., Tadokoro, S., Honda, S., Shiraga, M., Mizutani, H., Honda, M., Kurata, Y., Matsuzawa, Y. & Shattil, S.J. (1999) A mutation in the extracellular cysteine-rich repeat region of the β3 subunit activates integrins αIIbβ3 and αVβ3. *Blood*, **93**, 2559–2568.

Kunishima, S., Kashiwagi, H., Otsu, M., Takayama, N., Eto, K., Onodera, M., Miyajima, Y., Takamatsu, Y., Suzumiya, J., Matsubara, K., Tomiyama, Y. & Saito, H. (2011) Heterozygous ITGA2B R995W mutation inducing constitutive activation of the αIIbβ3 receptor affects proplatelet formation and causes congenital macrothrombocytopenia. *Blood*, **117**, 5479–5484.

Nurden, A.T. (2006) Glanzmann thrombasthenia. *Orphanet Journal of Rare Diseases*, **1**, 10.

Nurden, P. & Nurden, A.T. (2008) Congenital disorders associated with platelet dysfunctions. *Thrombosis and Haemostasis*, **99**, 253–263.

Nurden, A.T., Fiore, M., Nurden, P. & Pillois, X. (2011a) Glanznmann thrombasthenia: a review of ITGA2B and ITGB3 defects with emphasis on variants, phenotype variability, and mouse models. *Blood*, **118**, 5996–6005.

Nurden, A.T., Pillois, X., Fiore, M., Heilig, R. & Nurden, P. (2011b) Glanzmann thrombasthenia-like syndromes associated with macrothrombocytopenias and mutations in the gene encosing the αIIbβ3 integrin. *Seminars in Thrombosis and Hemostasis*, **37**, 698–706.

Schaffner-Reckinger, E., Salsmann, A., Debili, N., Bellis, J., Demey, J., Vainchenker, W., Ouwehand, W.H. & Kieffer, N. (2009) Overexpression of the partially activated αIIbβ3D723H integrin salt bridge mutant downregulates RhoA activity and induces microtubule-dependent proplatelet-like extensions in Chinese hamster ovary cells. *Journal of Thrombosis and Haemostasis*, **7**, 1207–1217.

Shattil, S.J., Cunningham, M. & Hoxie, J.A. (1987) Detection of activated platelets in whole blood using activation-dependent monoclonal antibodies and flow cytometry. *Blood*, **70**, 307–315.

ELSEVIER

Experimental Hematology

Experimental Hematology 2012;40:751–760

Regulation of hematopoietic stem cells using protein transduction domain–fused Polycomb

Teruyuki Kajiume[a], Yasuhiko Sera[a], Yumi Kawahara[b], Masaya Matsumoto[b], Takahiro Fukazawa[b], Takeshi Imura[b], Louis Yuge[b], and Masao Kobayashi[a]

[a]*Department of Pediatrics, Graduate School of Biomedical Sciences, Hiroshima University, Hiroshima, Japan;* [b]*Division of Bio-Environmental Adaptation Sciences, Graduate School of Health Sciences, Hiroshima University, Hiroshima, Japan*

(Received 9 November 2011; revised 7 May 2012; accepted 16 May 2012)

The Polycomb-group complex is a chromatin regulatory factor that is classified into two different complexes: Polycomb repressive complex 1 and 2. Components of Polycomb repressive complex 1 are involved in the self-renewal of hematopoietic stem cells. Bmi1, one of these components, maintains the immaturity of neural and cancer stem cells as well as that of hematopoietic stem cells. We constructed recombinant protein transduction domain (PTD)-Polycomb proteins and transduced them into murine bone marrow (BM) cells. We designed and fused the PTD–protein transduction domain to three proteins (i.e., green fluorescent protein, Bmi1, and Mel18). Murine BM cells were incubated for 48 h and each PTD-Polycomb protein was added. Then, we analyzed the function of hematopoiesis using the colony assay and transplantation. BM cells exposed to PTD-Bmi1 showed an increased number of colonies. In contrast, BM cells exposed to PTD-Mel18 or to both proteins showed a decreased number of colonies. Hematopoietic cells derived from PTD-Bmi1–transduced BM cells were significantly increased in the peripheral blood at 6 weeks after transplantation. Moreover, 80% of mice transplanted with PTD-Bmi1–transduced BM cells died at 8 to 24 weeks after transplantation. However, only a few early deaths were observed in the mice transplanted with BM cells exposed to both PTD-Bmi1 and PTD-Mel18. We expect that hematopoietic stem cells could proliferate after transduction with PTD-Bmi1, but this may generate undesirable effects, e.g., tumorigenesis. Thus, Bmi1 and Mel18 have opposing functions and are present in distinct complexes. © **2012 ISEH - Society for Hematology and Stem Cells. Published by Elsevier Inc.**

Polycomb-group genes encode molecules that form the Polycomb-group complex, which is involved in the methylation and ubiquitylation of histones [1–4]. The Polycomb-group complex is a chromatin regulatory factor that includes two types of complexes: Polycomb repressive complex (PRC) 1 and PRC2 [5–9]. The components of PRC1 are involved in the self-renewal of hematopoietic stem cells (HSCs) in mammals [10–14]. Bmi1, one of these components, maintains the immaturity of neural and cancer stem cells as well as that of HSCs [15–20]. However, *BMI1* is also involved in the malignancy of cancer cells, and a relationship between *BMI1* expression and prognosis has been reported for various types of tumors [21–24]. *BMI1* is related to tumorigenesis as well as to the immaturity of cells.

The Mel18 protein is composed of 342 amino acids, and the *N*-terminal region of the 102nd amino acid, which includes the really interesting new gene (RING) finger motif and shares 93% homology with the Bmi1 protein [25]. In addition, the secondary structure of this region shows a high homology with the Mel18 and Bmi1 proteins. Many studies have shown that *mel18*, which has 90% homology to *bmi1*, has opposing functions to *bmi1* [26–29]. We previously reported that *mel18* is necessary for the differentiation of murine HSCs, and not for their self-renewal, in experiments using knockout mice and gene knockdown with RNA interference (RNAi) [13]. This function of *mel18* is the opposite to that of *bmi1*. Moreover, we reported that *bmi1* and *mel18* act reciprocally in HSCs [14].

Offprint requests to: Teruyuki Kajiume, M.D., Ph.D., Department of Pediatrics, Graduate School of Biomedical Sciences, Hiroshima University, 1-2-3 Kasumi, Minami-ku, Hiroshima 734-8551, Japan; E-mail: kajiume@hiroshima-u.ac.jp

Supplementary data related to this article can be found online at http://dx.doi.org/10.1016/j.exphem.2012.05.005.

0301-472X/$ - see front matter.
http://dx.doi.org/10.1016/j.exphem.2012.05.005

In protein transduction, high molecular-weight target proteins are induced into cells by fusing them with peptides called protein transduction domains (PTDs), such as HIV tat and polyarginine [30,31]. An innovative study showed the induction of self-renewal in murine HSCs using a recombinant TAT-HoxB4 protein [32]. Furthermore, Zhou et al. recently reported the successful establishment of induced pluripotent stem cells using a recombinant protein fused with polyarginine [33].

In this study, we constructed recombinant PTD-Polycomb proteins and transduced them into murine HSCs. Although the transduced HSCs showed potential symptoms of tumorigenesis, our results indicate that the transduced Bmi1 or Mel18 may regulate the self-renewal or differentiation of HSCs without gene transduction.

Materials and methods

Mice

We used 5- to 8-week-old C57BL/6 mice (Ly5.1 or Ly5.2). Ly5.1 mice were obtained from The Sankyo Labo Service Corporation (Tokyo, Japan). All mice were bred and maintained in the animal facility at Hiroshima University.

Cells

Collection of murine bone marrow cells. Bone marrow (BM) was flushed from the medullary cavities of murine bones using phosphate-buffered saline.

Murine erythroleukemia cells. Murine erythroleukemia (MEL) cells were cultured in RPMI-1640 medium supplemented with 10% fetal bovine serum and 2% penicillin/streptomycin.

Preparation of the Polycomb *expression vector, protein extraction, and purification*

Full-length *bmi1* and *mel18* complementary DNAs were generated by real-time reverse transcriptase polymerase chain reaction (PCR) (ReverTra Ace and KOD plus; TOYOBO Co., Ltd., Osaka, Japan) from messenger RNA extracted from murine BM cells. Restriction enzyme sites were created on both ends of the PCR primers. To generate recombinant proteins that could penetrate the plasma membrane, we designed and fused a TAT peptide to the *N*-terminus or a polyarginine protein transduction domain to the *C*-terminus of three proteins (i.e., green fluorescent protein [GFP], Bmi1, and Mel18). The TAT and the polyarginine peptides enabled the recombinant proteins to enter the cells and allowed their translocation into the nucleus. *GFP*, *bmi1*, and *mel18* complementary DNAs were cloned into the pET47 expression plasmid (Merck KGaA, Darmstadt, Germany). The plasmids were transformed into *Escherichia coli* BL21 (DE3). Cells were grown in LB medium with kanamycin at 37°C using the Overnight Express Autoinduction System (Merck). His-tagged proteins were purified using TALON metal affinity resin (BD Biosciences, San Jose, CA, USA) according to the manufacturer's instructions.

Addition of PTD-Polycomb proteins

We added 20 ng/mL solution of the human flt3 ligand (PeproTech, London, UK) and human thrombopoietin (Kirin Brewery Co., Tokyo, Japan) to Dulbecco's modified Eagle's medium containing a supplement (StemPro 34; Invitrogen Inc., San Diego, CA, USA). The initial concentration of BM cells was 1.0×10^6 cells/mL. The culture plates were incubated at 37°C for 48 h in a humidified atmosphere with 5% CO_2. Each PTD-Polycomb protein was added at a final concentration of 50 nM. We introduced each PTD-Polycomb protein into our cell cultures every 6 h.

Flow cytometry analysis

To analyze the primitive hematopoietic cells, the collected cells were labeled with an antibody cocktail consisting of biotinylated anti-Gr1, anti-Mac1, anti-B220, anti-CD4, anti-CD8, and anti-Ter119 mouse antibodies. The cells were stained with phycoerythrin-conjugated anti-Sca1, allophycocyanin-conjugated anti–c-Kit, and streptavidin-conjugated peridinin-chlorophyll-protein complex. All antibodies were purchased from BD Pharmingen (San Diego, CA, USA). Dead cells stained with propidium iodide were excluded from the analysis. Flow cytometry analysis was performed on a FACSCaliber system (BD Biosciences, Bedford, MA, USA).

Western blot analysis

The MEL cells that were exposed to PTD-Polycomb proteins were separated into the nuclear and cytosolic fractions. For fractionation, a Nuclear/Cytosol Fractionation Kit (BioVision Inc., Mountain View, CA, USA) was used according to the manufacturer's protocol.

After 48 h of coculturing MEL cells with PTD-Polycomb proteins, His-tagged Polycomb proteins were extracted using TALON metal affinity resin (BD Biosciences). Cell extracts were used as samples for the pull-down assays.

Protein extracts were subjected to sodium dodecyl sulfate polyacrylamide gel electrophoresis and immunoblotting. The blot was removed from the transfer apparatus and blocked overnight at 4°C in Tris-buffered saline-Tween 20. The blot was washed three times in Tris-buffered saline-Tween 20 after the overnight incubation. We used the following primary antibodies: mouse monoclonal antibodies against Ring1 and Bmi1 (Millipore Corporation, Billerica, MA, USA), a goat polyclonal antibody against Mel18 (Abcam, Cambridge, UK), and a mouse monoclonal antibody against the 6x His synthetic peptide (Abcam). Chemiluminescence was detected using ECL plus Western blotting detection reagents (GE Healthcare UK Ltd, Little Chalfont, UK).

Quantitative reverse transcriptase PCR

To analyze the influence of PTD-Polycomb proteins, we performed reverse transcription using ExScript reverse transcriptase and SYBR Premix Ex Taq (TAKARA BIO Inc., Shiga, Japan) according to manufacturer's protocol. Real-time PCR was used for the quantitative analysis of gene expression (Opticon; Bio-Rad Laboratories, Hercules, CA, USA). The following specific primers were used: mouse *cdkn2a* (ink4a), sense primer 5′-CGA TTC AGG TGA TGA TGG-3′ and antisense primer 5′-CAG CGT GTC CAG GAA GC-3′; and mouse *actB*, sense primer 5′-CAT CCG TAA AGA CCT CTA TGC CAA C-3′ and antisense primer 5′-ATG GAG CCA CCG ATC CAC A-3′.

Methylcellulose colony assay

In vitro colony-forming cell activity was assessed by performing a methylcellulose colony assay. BM cells (1000 cells/well) were cultured in a methylcellulose medium containing various

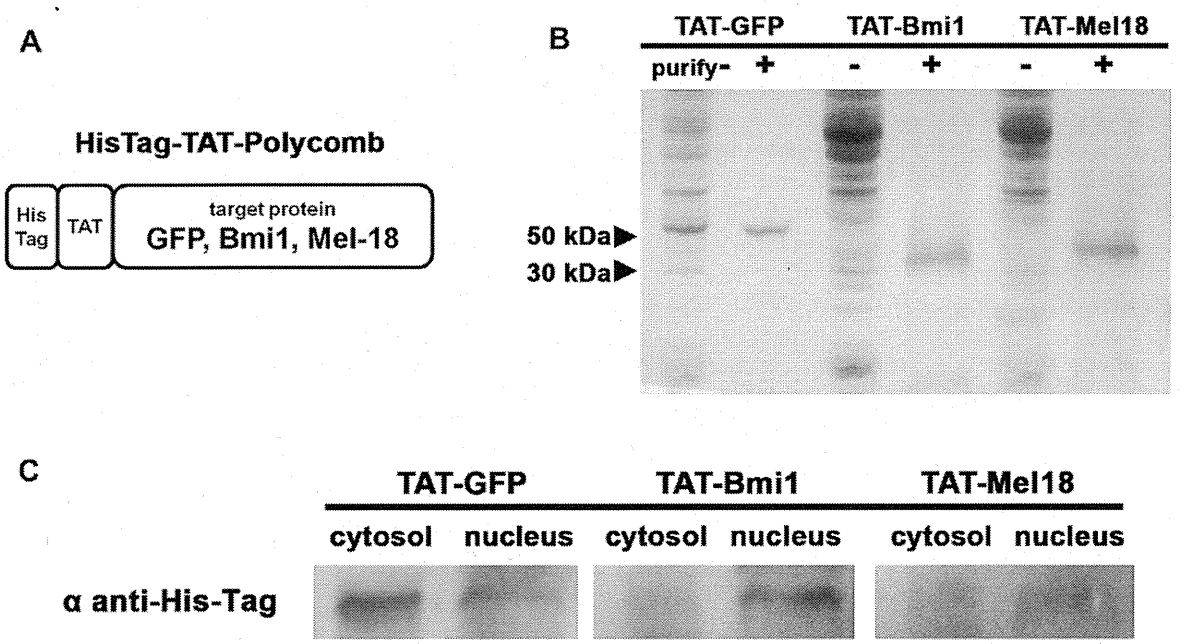

Figure 1. Preparation of recombinant TAT-Polycomb proteins. (**A**) *bmi1*, *mel18*, and *GFP* genes were fused with a HisTag and TAT at their *N*-terminus. (**B**) The recombinant TAT-Polycomb proteins were purified. Proteins were separated using sodium dodecyl sulfate polyacrylamide gel electrophoresis, and the polyacrylamide gel was stained with Coomassie brilliant blue. (**C**) Purified TAT-Polycomb was added to cultures of MEL cells. The MEL cells were separated into the nuclear and cytosolic fractions. GFP was detected more often in the cytosol than in the nucleus. Bmi1 and Mel18 were detected exclusively in the nucleus.

cytokines (Methocult GF M3434; StemCell Technologies, Vancouver, BC, Canada). The culture plates were incubated at 37°C for 7 days in a humidified atmosphere with 5% CO_2. A colony was defined as a group of >50 cells. Erythroid, myeloid, and mixed erythroid-myeloid colonies were counted using an inverted microscope. A secondary colony-forming cell assay was performed by replating aliquots of the cells obtained by harvesting complete primary colonies. The secondary colonies were counted after an additional week of incubation.

In vivo BM transplantation assay

We performed a transplantation experiment in which the recipient mice were F1 hybrids of Ly5.1 and Ly5.2 mice. Donor and competitor cells (2.0×10^5 cells each) were intravenously transplanted into F1 recipients that were lethally irradiated with a dose of 9 Gy (rate, 1 Gy/min). Four donor and four competitor mice were used for each marrow transplantation experiment. Eight to 12 mice were used as the recipient mice for each BM transplantation experiment. For the donor Ly5.2 cells, each cell was exposed to PTD-Polycomb proteins before being analyzed, and the competitor Ly5.1 cells were exposed to PTD-GFP. Peripheral blood samples were collected from the recipient mice every 4 weeks after transplantation. To distinguish between the 2 competing transplant cell populations, we stained the cells with phycoerythrin-conjugated anti-Ly5.1 and allophycocyanin-conjugated anti-Ly5.2. All antibodies were purchased from Abcam.

Statistical analysis

Data are presented as the mean ± standard error, unless otherwise stated. Student's *t* test was applied. Differences of $p < 0.05$ were considered statistically significant.

Results

Preparation of recombinant PTD-Polycomb proteins

We manipulated the *bmi1*, *mel18*, and *GFP* genes such that they were fused to a HisTag and TAT at their *N*-terminus or a polyarginine at their *C*-terminus and inserted the designed genes into pET plasmids (Fig. 1A, Supplementary Figure E1A; online only, available at www.exphem.org). These pET plasmids were transformed into DE3 cells, and the recombinant PTD-Polycomb proteins were purified as described previously (Fig. 1B, Supplementary Figure E1B; online only, available at www.exphem.org). Most GFP proteins form dimers because of their high concentrations. Purified PTD-Polycomb was added to cultures of MEL cells. The MEL cells were separated into their nuclear and cytosolic fractions after 6 h of culture, and the distribution of the PTD-Polycomb proteins was analyzed. GFP was detected more often in the cytosol than in the nucleus. Bmi1 and Mel18 were detected exclusively in the nucleus (Fig. 1C, Supplementary Figure E1C; online only, available at www.exphem.org). These results indicate that PTD-Polycomb proteins can be translocated to the nucleus after their addition to the culture medium.

Flow cytometry profile of recombinant TAT-Polycomb protein-transduced murine BM cells

We performed flow cytometry analysis of murine BM cells exposed to recombinant TAT-Polycomb proteins for 48 h.

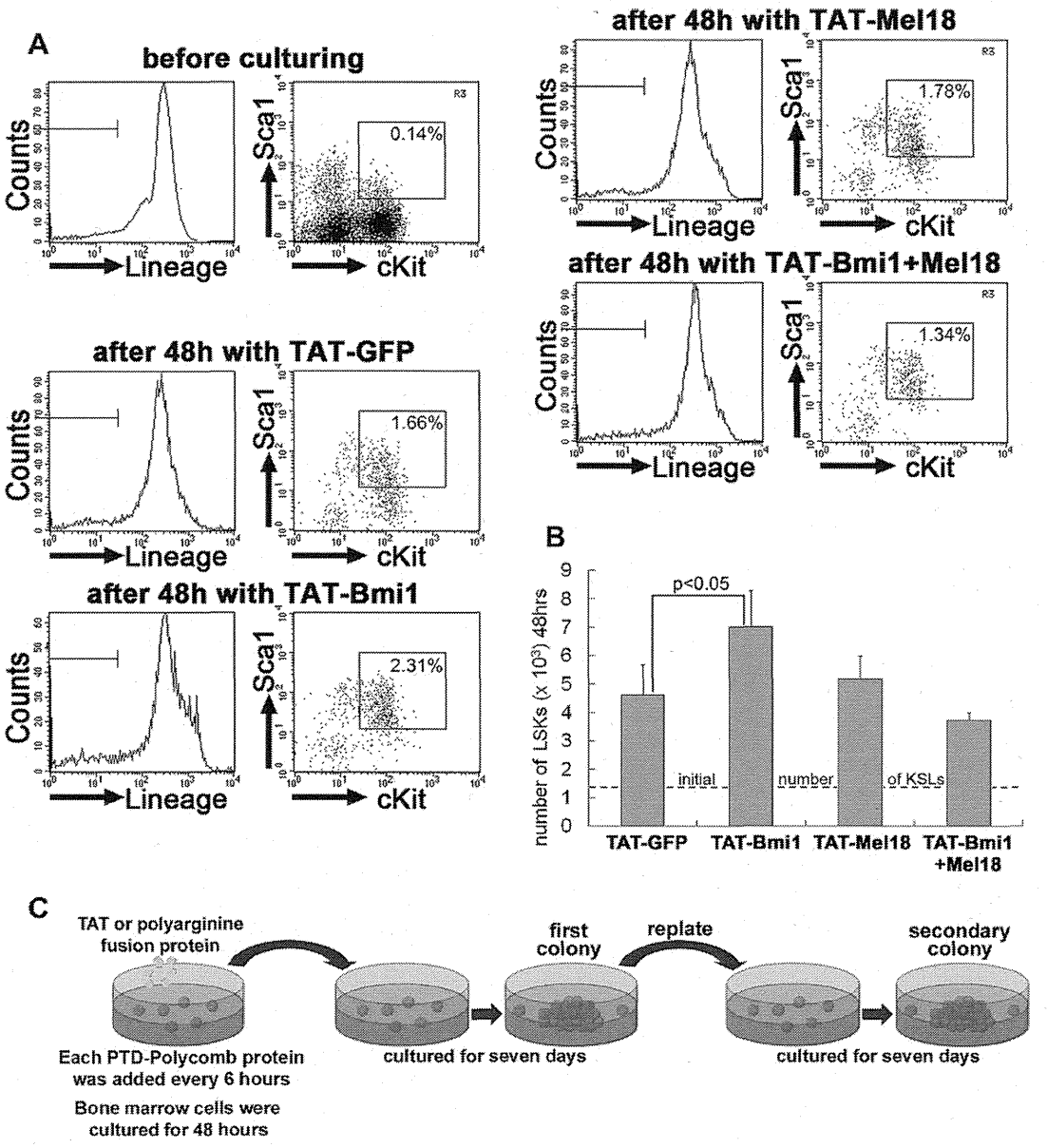

Figure 2. In vitro colony assay of recombinant TAT-Polycomb protein-transduced murine bone marrow (BM) cells. (**A**) The initial ratio of LSK cells from BM of fresh mice was ~0.14%. The ratio of LSK cells was increased when TAT-Bmi1 was added in BM cells and cultured for 48 h compared with the other recombinant proteins. (**B**) In comparison with the total cell number, the number of LSK cells was significantly increased following the addition of TAT-Bmi1. In addition to TAT-Mel18 alone, or the addition of both TAT-Bmi1 and TAT-Mel18, the number of LSK cells was not significantly increased compared with TAT-GFP. (**C**) Recombinant TAT-Polycomb proteins were added during the first 48 h of culturing. A methylcellulose colony assay was performed using marrow cells to which each protein was added. Then, the secondary colony-forming potential of the cells was assayed.

Because the lineage marker–negative, Sca-1–positive, and c-Kit–positive (LSK) cells possess the highest long-term multilineage reconstitution activity [34,35], we used this population for these experiments. The ratio of LSK cells from murine BM was 0.14%. The ratio of LSK cells increased when TAT-Bmi1 was added to BM cells and cultured for 48 h compared to the addition of other fused proteins (Fig. 2A). The initial concentration of BM cells was 1.0×10^6 cells/mL; the number of LSK cells was significantly increased after the addition of TAT-Bmi1. In addition to TAT-Mel18 alone, or the addition of both TAT-Bmi1 and TAT-Mel18, the number of LSK cells was not increased compared with TAT-GFP (Fig. 2B).

In vitro colony assay of recombinant TAT-Polycomb protein-transduced murine BM cells

We performed a secondary colony assay to assess primitive hematopoiesis [13,14]. The secondary colony-forming

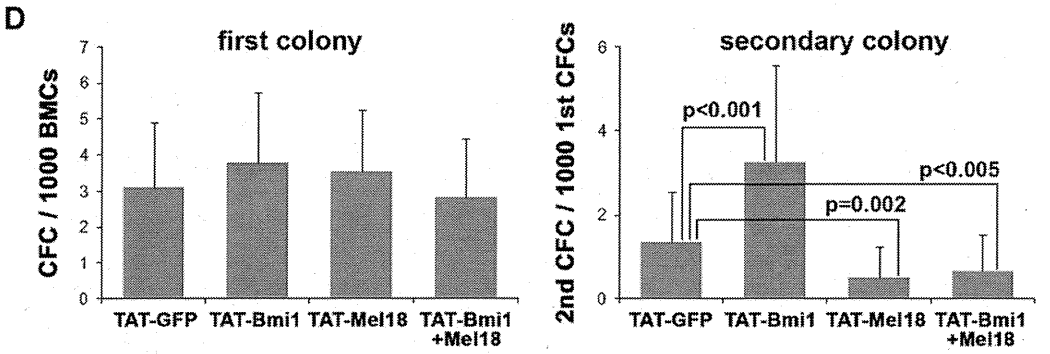

Figure 2. (*Continued*) (**D**) There was no significant difference in primary colony-forming potential between the recombinant proteins. However, BM cells exposed to recombinant TAT-Bmi1 showed an increased number of secondary colonies. In contrast, BM cells exposed to recombinant TAT-Mel18 or to both proteins showed a decreased number of secondary colonies.

potential of murine BM cells exposed to recombinant TAT-Polycomb proteins at a final concentration of 50 nM for 48 h was assayed (Fig. 2C). There were no significant differences in the primary colony-forming potential between the recombinant proteins. There was no significant difference in the classification of the colonies (e.g., colony-forming unit granulocyte-macrophage, burst-forming unit erythroid), even when TAT-Polycomb protein was added. However, BM cells exposed to recombinant TAT-Bmi1 showed an increased number of secondary colonies. In contrast, BM cells exposed to recombinant TAT-Mel18 or to both recombinant proteins showed a decreased number of secondary colonies (Fig. 2D). Similar results were obtained for recombinant polyarginine-Polycomb (Supplementary Figure E2; online only, available at www.exphem.org). These results suggest that Mel18 may attenuate the potential of Bmi1 to increase the formation of secondary colonies.

In vivo BM transplantation assay of recombinant TAT-Polycomb protein-transduced murine BM cells and tumorogenesis

Murine BM cells exposed to TAT-Polycomb for 48 h were transplanted into 9-Gy–irradiated mice. Hematopoietic cells derived from TAT-Bmi1–transduced BM cells were significantly increased in the peripheral blood at 6 weeks after transplantation (Fig. 3A). The effect of Bmi1 was attenuated after the transplantation of BM cells exposed to both TAT-Bmi1 and TAT-Mel18. Figure 3B shows the flow cytometry analysis of peripheral blood cells from these transplanted mice at 6 weeks after transplantation. Because 80% of mice transplanted with TAT-Bmi1–transduced BM cells died at 8 to 24 weeks after transplantation, we could not perform long-term engraftment analysis. However, only a few early deaths were observed in mice transplanted with BM cells exposed to both TAT-Bmi1 and TAT-Mel18 (Fig. 4A). It is possible that the mice transplanted with BM cells exposed to TAT-Bmi1 died because of cancer, such as leukemia, because *BMI1* is also involved in the malignancy of cancer cells [21–24]. However, we were not able to analyze this before the mice died. Murine BM cells were exposed to TAT-Polycomb for only 48 h and then cell culturing was continued for 8 weeks with cytokines. However, we detected no morphological malignancies in the cells (Fig. 4B). During cell culturing for 8 weeks, the number of Bmi1-exposed cells was expanded by approximately 500 times the original number of cultured cells (Fig. 4C). Although we could not prove the malignancy of these cells, this phenomenon could represent the proliferation of malignant cells.

Regulation of target gene expression by recombinant TAT-Polycomb proteins in vitro

We added each TAT-fusion protein to MEL cells every 6 h until 48 h and examined cell proliferation. Cell proliferation increased after the addition of either Bmi1 or Mel18, as assessed by cell growth (Fig. 5A). The cell cycle inhibitory gene *ink4a/arf* is a target of Bmi1. To analyze whether the transduced recombinant Polycomb proteins regulate the expression of their target genes, we performed real-time reverse transcriptase PCR on MEL cells that were cultured for 48 h with TAT-Polycomb at a final concentration of 50 nM. The expression of these genes was inhibited in MEL cells exposed to TAT-Polycomb (Fig. 5B).

Bmi1 and Mel18 are present in distinct complexes

We previously demonstrated that only a small number of hematopoietic cells simultaneously express *bmi1* and *mel18* [14]. In the present study, we performed a pull-down assay with HisTag to analyze whether Polycomb-group complexes includes both Bmi1 and Mel18.

We did not detect Bmi1, Mel18, or Ring1A in the pull-down assays of protein extracts from MEL cells exposed to TAT-GFP for 6 h using a HisTag-specific resin. However, in the pull-down assay of MEL cells exposed to TAT-Bmi1, Bmi1, and RINGA1A were detected together with a small quantity of Mel18. In contrast, Bmi1 was not detected in MEL cells exposed to TAT-Mel18 (Fig. 5C). These results suggest that PRC1 includes either Bmi1 or Mel18 (Fig. 5D).

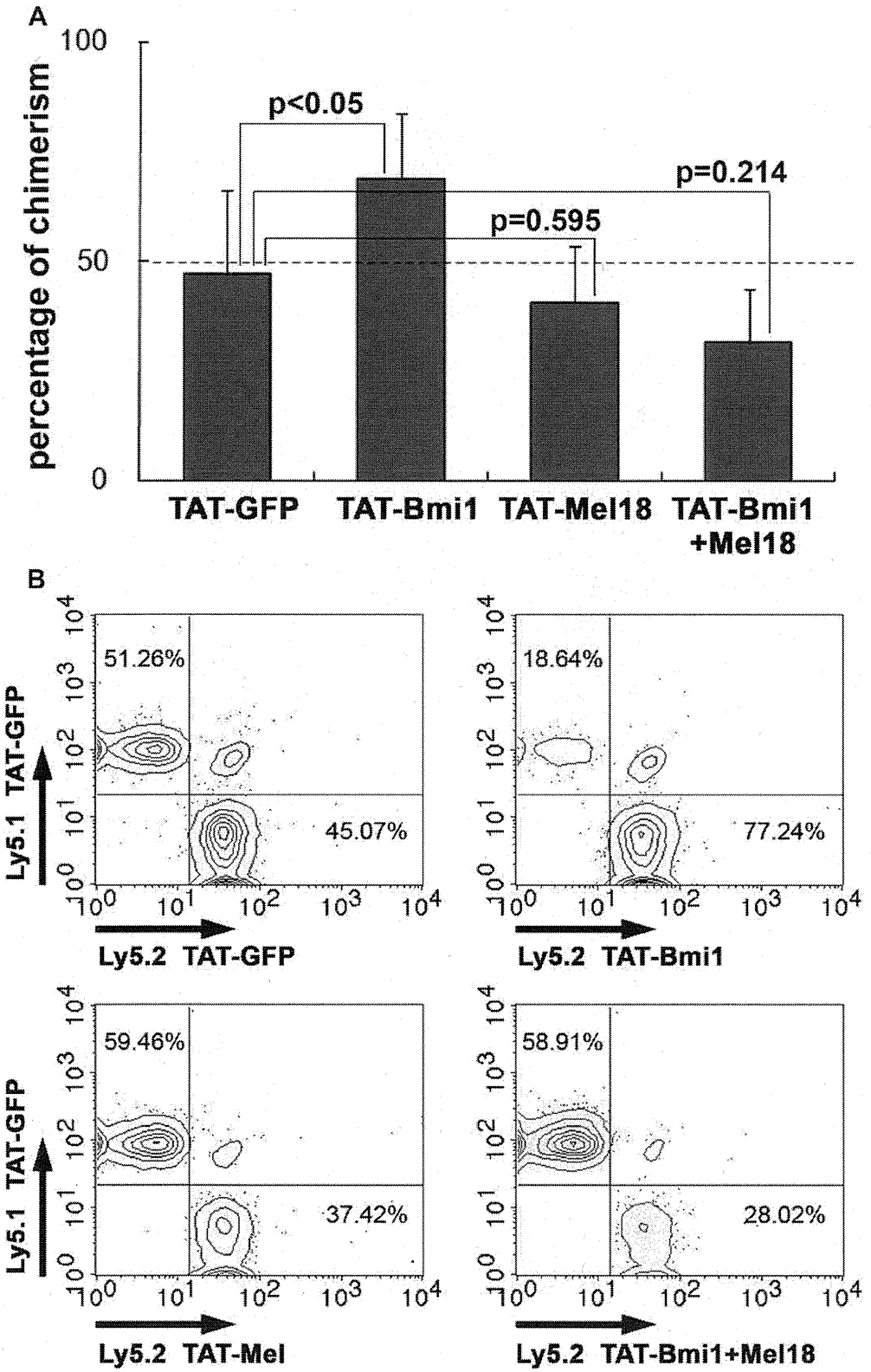

Figure 3. In vivo BM transplantation assay of recombinant TAT-Polycomb protein-transduced murine BM cells. (**A**) Hematopoietic cells derived from TAT-Bmi1–transduced BM cells were significantly increased in the peripheral blood at 6 weeks after transplantation. The effect of Bmi1 was attenuated following the transplantation of BM cells exposed to both TAT-Bmi1 and TAT-Mel18. (**B**) Flow cytometry profiles of peripheral blood cells from transplanted mice at 6 weeks after transplantation.